Available online at www.sciencedirect.com
ScienceDirect
International Journal of Plasticity 24 (2008) 915–944
INTERNATIONAL JOURNAL OF Plasticity
www.elsevier.com/locate/ijplas

On the use of homogeneous polynomials to develop anisotropic yield functions with applications to sheet forming

Stefan Soare [a,*], Jeong Whan Yoon [b], Oana Cazacu [a,*]

[a] *University of Florida, Reef, 1350 N. Poquito Road, Shalimar, FL 32579, USA*
[b] *Material Science Division, Alcoa Technical Center, 100 Technical Drive, Alcoa Center, PA 15069, USA*

Received 21 May 2007; received in final revised form 27 July 2007
Available online 10 August 2007

Abstract

This paper investigates the capabilities of several non-quadratic polynomial yield functions to model the plastic anisotropy of orthotropic sheet metal (plane stress). Fourth, sixth and eighth-order homogeneous polynomials are considered. For the computation of the coefficients of the fourth-order polynomial an improved set of analytic formulas is proposed. For sixth and eighth-order polynomials the identification uses optimization. Simple constraints on the optimization process are shown to lead to real-valued convex functions. A general method to extend the above plane stress criteria to full 3D stress states is also suggested. Besides their simplicity in formulation, it is found that polynomial yield functions are capable to model a wide range of anisotropic plastic properties (e.g., the Numisheet'93 mild steel, AA2008-T4, AA2090-T3). The yield functions have then been implemented into a commercial finite element code as constitutive subroutines. The deep drawing of square (Numisheet'93) and cylindrical (AA2090-T3) cups have been simulated. In both cases excellent agreement with experimental data is obtained. In particular, it is shown that non-quadratic polynomial yield functions can simulate cylindrical cups with six or eight ears. We close with a discussion on earing and further examples.

Keywords: Orthotropic sheet metal; Polynomial yield function; Earing

* Corresponding authors. Tel.: +1 850 833 9350; fax: +1 850 833 9366.
E-mail addresses: soare@reef.ufl.edu (S. Soare), cazacu@reef.ufl.edu (O. Cazacu).

0749-6419/$ - see front matter © 2007 Elsevier Ltd. All rights reserved.
doi:10.1016/j.ijplas.2007.07.016

1. Introduction

Within the framework of phenomenological plasticity, recent investigations on the prediction of limit strains during sheet stretching (e.g. Wu et al., 2003), and on the prediction of earing in cylindrical cups (e.g. Yoon et al., 2006), have confirmed the important role played in the numerical simulation of plastic deformation of rolled sheets by the accurate description of the initial plastic anisotropy of the sheet. In the cited papers this description was successfully achieved for both yielding and flow (r-value) properties by using the principal values-based anisotropic yield functions Yld96, Barlat et al. (1997) and Yld2004, Barlat et al. (2005). An account of a general method by which principal values-based anisotropic yield functions can be designed by using linear transformations on the stress tensor is given in Barlat et al. (2007).

In this paper we are concerned with yet another general method of describing the plastic anisotropy of a metalic sheet, a method based on homogeneous polynomials in the components of the stress tensor with respect to the symmetry axes. First, the material symmetry of a (cold) rolled sheet can be satisfactorily approximated as orthotropic, with the three orthogonal symmetry planes intersecting along the rolling direction (RD), transverse direction (TD, the direction in the plane of the sheet orthogonal to RD), and the direction normal to the plane of the sheet (ND). Then we shall consider an orthogonal Cartesian coordinate system xyz aligned with the RD, TD, and the ND, respectively. With respect to this coordinate system the components of the stress tensor will be denoted as usual, σ_x, σ_{xy}, etc. The orthotropic symmetry group of the material is then generated by the 180° degrees rotations about the x axis, call it Q_1, and about the y axis, call it Q_2. The necessary and sufficient condition for a yield function $f = f(\sigma_x, \sigma_y, \sigma_z, \ldots)$ to be orthotropic (i.e., be invariant with respect to the symmetry group) is then

$$f([Q_i]^{\mathrm{T}}[\sigma][Q_i]) = f([\sigma]), \quad i = 1, 2 \tag{1}$$

for any stress state $[\sigma]$. In Eq. (1), $[Q_i]$ and $[\sigma]$ are the matrices of the rotations and of the stress tensor with respect to the symmetry axes, and $[\cdot]^{\mathrm{T}}$ denotes the transposition operation. Thus, the yield function is orthotropic if and only if it satisfies the relations:

$$f(\sigma_x, \sigma_y, \sigma_z, -\sigma_{xy}, \sigma_{xz}, -\sigma_{yz}) = f(\sigma_x, \sigma_y, \sigma_z, \sigma_{xy}, \sigma_{xz}, \sigma_{yz}) \tag{2}$$

$$f(\sigma_x, \sigma_y, \sigma_z, -\sigma_{xy}, -\sigma_{xz}, \sigma_{yz}) = f(\sigma_x, \sigma_y, \sigma_z, \sigma_{xy}, \sigma_{xz}, \sigma_{yz}) \tag{3}$$

for any stress state. In particular, a plane stress yield function is orthotropic if and only if

$$f(\sigma_x, \sigma_y, -\sigma_{xy}) = f(\sigma_x, \sigma_y, -\sigma_{xy}) \tag{4}$$

for any plane stress state.

Recognizing the limitations of his quadratic criterion, Hill (1950, p. 330), suggests the use of a general homogeneous polynomial in the form:

$$P_n^{2\mathrm{D}}(\sigma) = \sum_{i+j+2k=n} a_{ijk}\sigma_x^i\sigma_y^j\sigma_{xy}^{2k} \tag{5}$$

as yield function for plane stress states. The integers i, j, k are all non-negative. Since the shear component of the stress appears only at even powers, from (4) it follows that the above function is orthotropic. We note that only symmetric criteria (i.e, $f(-[\sigma]) = f([\sigma])$) are considered in this work, and thus the homogeneity degree n is always even in (5). With few exceptions (e.g. Gotoh, 1977), this approach for modeling orthotropic symme-

try, using directional yield strength and r-value data for material characterization, has received little attention. One possible reason might be that not every such polynomial is a positive convex function, one fundamental property of a yield function. Without special precautions, it is indeed difficult to find a convex yield surface within the class of functions of type (5) when all is given is a curve on the surface (the directional yield strength) and relations between the components of the surface gradient along that curve (the directional r-value). It should be noted that fourth and sixth-order polynomials have also been used in dual formulations as strain rate potentials, e.g. Arminjon et al. (1994), Savoie and MacEwen (1995), Zhou et al. (1998). For a recent review of the method based on strain rate potentials the reader is referred, for example, to the work of Dawson et al. (2003). With this approach, the identified potential surface has in general greater chances of being real-valued and convex due to the fairly large data set available and its spatial distribution. However, loss of convexity (fish-tails) has been reported even in this case, Arminjon et al. (1994), Savoie and MacEwen (1995). Here we study polynomials of order four, six and eight in the stress space and we show that simple constraints on the identification process lead aposteriori to convex yield surfaces, determined solely from yield strength and r-value data. We also propose 3D orthotropic extensions that preserve the convexity and do not need extensive out-of-plane data sets for identification.

In this work, the uniaxial yield strength at an angle θ from RD is denoted σ_θ, and this data set is normalized with the yield strength along the RD, i.e., $\bar{\sigma}_\theta := \sigma_\theta/\sigma_0$. The equibiaxial yield strength (plane stress tensile test where $\sigma_x = \sigma_y$, $\sigma_{xy} = 0$) is denoted σ_b, and its normalized value $\bar{\sigma}_b := \sigma_b/\sigma_0$. The r-value at an angle θ from rolling, defined as the ratio of the transverse strain rate to the thickness strain rate in the uniaxial at an angle θ from RD tensile test, is denoted r_θ. Finally, we will also use the biaxial r-value, r_b, defined as the ratio of the transverse to rolling strain rates from an equibiaxial test.

2. Convexity

Twice continuously differentiable functions are convex if and only if they have a positive semi-definite hessian. For first order homogeneous functions defined on $\mathbb{R}^2$ this condition takes a particularly simple form, Shephard (1968), or Groemer (1996). Let us first notice that if $f : \mathbb{R}^n \to \mathbb{R}_+$ is a first-order positive homogeneous function, then it is uniquely determined by its restriction to the unit sphere (its support function) denoted from now on by h:

$$f(x) = f(\|x\|x/\|x\|) = \|x\|f(x/\|x\|) = \|x\|h(u)$$

where $\boldsymbol{u} = \boldsymbol{x}/\|\boldsymbol{x}\|$, and $\|\boldsymbol{x}\|$ denotes the Euclidean norm of $\boldsymbol{x} \in \mathbb{R}^n$. When $n = 2$, the unit sphere becomes the unit one-dimensional circle. Associating with this circle a polar angle, say $\omega \in [0,2\pi)$, the support function h can be viewed as defined on a 1D interval h: $[0, 2\pi] \to R_+$, $h = h(\omega)$. We then have

Lemma 1. *If $f : \mathbb{R}^2 \to \mathbb{R}_+$ is first-order positive homogeneous, two times continuously differentiable, then f is convex if and only if its support function h satisfies*

$$h'' + h \geqslant 0 \tag{6}$$

Proof. Indeed, writing the hessian H of the function f in polar coordinates (r, ω) associated with Cartesian coordinates (x, y), and taking into account the first-order homogeneity of f, i.e., $f(r, \omega) = rh(\omega)$, we obtain

$$H[v, v] = (H : v) \cdot v = \frac{[h''(\omega) + h(\omega)]}{r} (v_1 \cos\omega - v_2 \sin\omega)^2$$

for any vector $v = [v_1, v_2]^T$. We then have $H[v, v] \geqslant 0$, if and only if Eq. (6) holds true. □

For first-order positive homogeneous functions defined on spaces of higher dimensions than two, a simple convexity equation like (6) is no longer available. However, it can be easily shown that every such function (and in general, any function) is convex if and only if its restriction to any two-dimensional hyperplane is convex. In particular, for plane stress cases where the yield surface is embedded in $\mathbb{R}^3$ we have.

Lemma 2. *If $f : \mathbb{R}^3 \to \mathbb{R}_+$ is first-order positive homogeneous, two times continuously differentiable, then f is convex if and only if its support function h satisfies inequality (6) along any plane section through the unit sphere S^2.*

Proof. In the case of a first-order homogeneous function of the general form

$$f(\sigma_x, \sigma_y, \sigma_{xy}) := [P_n(\sigma_x, \sigma_y, \sigma_{xy})]^{1/n} \tag{7}$$

with P_n a homogeneous polynomial of degree n, inequality (6) becomes

$$(n^2 P_n^{2-1/n})^{-1} [n^2 P_n^2 - (n-1)(P_n')^2 + nP_n P_n''] \geqslant 0 \quad (\forall)\omega \in [0, 2\pi) \tag{8}$$

and the conditions for f to be a real-valued convex function are then

$$P_n > 0 \quad \text{and} \quad n^2 P_n^2 - (n-1)\left(P_n'\right)^2 + nP_n P_n'' \geqslant 0 \quad (\forall)\omega \in [0, 2\pi) \tag{9}$$

for any plane section through the unit sphere. In practice, for the polynomial type criteria discussed in this paper it is sufficient to enforce these inequalities only along a discrete set of meridians and parallels of the unit sphere. Although we do not have a general proof for this assertion, this was always the case for fourth, sixth and eighth-order polynomials. □

3. Fourth-order polynomial criterion for plane stress states

With respect to the symmetry axes, the orthotropic fourth-order polynomial takes the form

$$P_4^{2D} = a_1\sigma_x^4 + a_2\sigma_x\sigma_y + a_3\sigma_x^2\sigma_y^2 + a_4\sigma_x\sigma_y^3 + a_5\sigma_y^4 + (a_6\sigma_x^2 + a_7\sigma_x\sigma_y + a_8\sigma_y^2)\sigma_{xy}^2 + a_9\sigma_{xy}^4 \tag{10}$$

It has been first considered by Gotoh (1977) who also proposed explicit formulas in terms of both yield strength and r-value data for its coefficients. However, Gotoh's direct approach for coefficient identification can often lead to an unbalanced overall characterization of the directional yield strength or r-value (it can exactly describe four data points but in the same time can have a big overall error), and offers no precautions with respect to the convexity of the yield surface. In this section we propose changes to Gotoh's identification

program, changes that still keep the formulas for coefficients explicit while balancing the overall error in prediction and improving upon the convexity of the yield surface. The superscript 2D in Eq. (10) will be dropped from now on since in this section only the plane stress case will be dealt with.

3.1. Bounds on coefficients and data

The five coefficients a_i, $i = 1, \ldots, 5$, describing the intersection of the yield surface with the biaxial plane (σ_x, σ_y) are determined using the yield strength data $\bar{\sigma}_0(=1), \bar{\sigma}_{90}, \bar{\sigma}_b$, and flow data r_0, r_{90}. Thus we have

$$a_1 = 1, \quad a_5 = 1/\bar{\sigma}_{90}^4 \tag{11}$$

$$a_2 = -4r_0/(1+r_0), \quad a_4 = 4a_5 r_{90}/(1+r_{90}) \tag{12}$$

$$a_3 = (1/\bar{\sigma}_b^4) - (a_1 + a_2 + a_4 + a_5) \tag{13}$$

The question is then under what conditions the yield curve in the biaxial plane is real and convex. Since $\bar{\sigma}_0, \bar{\sigma}_{90}$, and r_0, r_{90} must be accurately predicted, the only variable left is the coefficient a_3, or equivalently, from (13), the biaxial yield strength $\bar{\sigma}_b$. Thus we assume that a_1, a_2, a_4, and a_5 are computed according to Eqs. (11) and (12). The restriction of P_4 to the unit circle in this plane is

$$P_4(\omega) = a_1 \cos^4\omega + a_2 \cos^3\omega \sin\omega + a_3 \cos^2\omega \sin^2\omega + a_2 \cos^4 \cos\omega \sin^3\omega + a_5 \sin^4\omega \tag{14}$$

The restriction of the yield surface to the biaxial plane is then real-valued if

$$a_3 > \sup_{\omega\in(0,\pi)\setminus\pi/2} [-(a_1/t^2 + a_2/t + a_4 t + a_5 t^2)] =: Q \tag{15}$$

where $t := \tan(\omega)$. Using (13), the above inequality is rewritten as a bound for the biaxial yield strength data point

$$1/\bar{\sigma}_b^4 > Q + a_1 + a_2 + a_4 + a_5 \tag{16}$$

The restriction of the yield surface to the biaxial plane is convex if and only if the second inequality in (9) is satisfied. Here it takes the form

$$Aa_3^2 + Ba_3 + C \geqslant 0 \quad (\forall)\omega \in [0, 2\pi) \tag{17}$$

where

$$\begin{aligned} A &:= -4\cos^2\omega \sin^2\omega \leqslant 0 \quad (\forall)\omega \in [0, 2\pi) \\ B &:= 4[2a_1 \cos^4\omega - (a_2 \cos^2\omega + a_4 \sin^2\omega)\cos\omega \sin\omega + 2a_5 \sin^4\omega] \\ C &:= 3[16a_1 a_5 \cos^2\omega \sin^2\omega + 8a_2 a_5 \cos\omega \sin^3\omega + 8a_1 a_4 \cos^3\omega \sin\omega \\ &\quad - (a_2 \cos^2\omega - a_4 \sin^2\omega)^2] \end{aligned} \tag{18}$$

The coefficients $A = A(\omega)$, $B = B(\omega)$, and $C = C(\omega)$ can be estimated for any $\omega \in [0,2\pi)$. For any fixed ω, Eq. (17) has in general two real solutions $x_1(\omega) \leqslant x_2(\omega)$, and for Eq. (17) to hold true for any ω we must have

$$M_1 := \max_{\omega\in[0,\pi/2)} x_1 \leqslant a_3 \leqslant \min_{\omega\in[0,\pi/2)} x_2 =: M_2 \tag{19}$$

Although formulas for M_1 and M_2 are difficult to obtain in explicit form, they can be estimated numerically with any degree of accuracy. Then, using Eq. (13), they can be further used to estimate the interval where the biaxial yield strength $\bar{\sigma}_b$ is allowed to vary in order to have a convex yield curve in the biaxial plane:

$$(M_2 + a_1 + a_2 + a_4 + a_5)^{-1/4} \leqslant \bar{\sigma}_b \leqslant (M_1 + a_1 + a_2 + a_4 + a_5)^{-1/4} \tag{20}$$

Inequalities (16) and (20) are necessary and sufficient conditions for the biaxial yield curve to be real-valued and convex. Next, we repeat the same argument as above and obtain conditions for three more curves on the yield surface to be real-valued and convex. The reasoning is elementary and it is outlined in Appendix 1. Here we just list these conditions.

The data points at $\theta = 45°$ from rolling, $\bar{\sigma}_{45}$ and r_{45}, are exactly matched if and only if the following two equations hold true

$$a_9 = \frac{(2/\bar{\sigma}_{45})^4 r_{45}}{1 + r_{45}} + B_1 > 0 \tag{21}$$

$$a_6 + a_7 + a_8 = \frac{(2/\bar{\sigma}_{45})^4}{1 + r_{45}} - 2B_1 =: B_5 \tag{22}$$

where

$$B_1 := a_1 + a_2 + a_3 + a_4 + a_5 = 1/\bar{\sigma}_b^4 \tag{23}$$

Then the yield curves in the planes $\sigma_y = 0$ and $\sigma_x = 0$ are real-valued and convex if and only if the following inequalities are met, respectively,

$$0 \leqslant a_6 \leqslant 6\sqrt{a_1 a_9}, \quad 0 \leqslant a_8 \leqslant 6\sqrt{a_5 a_9} \tag{24}$$

Finally, assuming Eq. (22) to hold true, the yield curve in the plane $\sigma_x = \sigma_y$ is real-valued and convex if and only if

$$\frac{-(5t + 8) + (3/2)t(t + 8)^{1/2}}{9t + 8} \leqslant r_{45} \leqslant t/2 - 1 \tag{25}$$

where we have denoted $t := (2/\bar{\sigma}_{45})^4 / B_1 = (2\bar{\sigma}_b/\bar{\sigma}_{45})^4$.

3.2. Identification procedure for Poly4

To complete the coefficient identification procedure, it remains to identify a_6 and a_8. Two more equations for a_6 and a_8 can be obtained by using data $\bar{\sigma}_\theta$ and r_θ at an angle θ from the rolling direction. This angle can be 15°, 30°, 60°, 75°, or 22.5°, 67.5°. In any case, the two new equations obtained from predicted $\bar{\sigma}_\theta$ and r_θ, respectively, are

$$c^2 a_6 + csa_7 + s^2 a_8 = B_6 \tag{26}$$

$$g_1 a_6 + g_3 a_7 + g_2 a_8 = B_7 \tag{27}$$

where $c := \cos^2\theta$, $s := \sin^2\theta$, and

$$g_1 := 2c(r_\theta - c + s), \quad g_2 := 2s(r_\theta - c - s), \quad g_3 := r_\theta + (c - s)^2 \tag{28}$$

$$B_6 := \left(\frac{1}{\bar{\sigma}_\theta^4} - B_2 - a_9 c^2 s^2\right)/(cs) \tag{29}$$

$$B_2 := a_1 c^4 + a_2 c^3 s + a_3 c^2 s^2 + a_4 c s^3 + a_5 s^4 \tag{30}$$

$$B_7 := (4a_9 c^2 s^2 - r_\theta B_3 - B_4)/(cs) \tag{31}$$

$$B_3 := 4a_1 c^3 + a_2 c^2(3s + c) + 2a_3 cs + a_4 s^2(s + 3c) + 4a_5 s^3 \tag{32}$$

$$B_4 := 4a_1 c^3 s + a_2 c^2(3s^2 + c^2) + 2a_3 cs(c^2 + s^2) + a_4 s^2(s^2 + 3c^2) + 4a_5 cs^3 \tag{33}$$

After substituting for a_7 from Eq. (22), which, coupled with Eq. (21) for a_9, assures exact predictions for $\bar{\sigma}_{45}$ and r_{45}, into Eqs. (26) and (27), we obtain

$$(c^2 - cs)a_6 + (s^2 - cs)a_8 = B_6 - B_5 cs \tag{34}$$

$$(g_1 - g_3)a_6 + (g_2 - g_3)a_8 = B_7 - B_5 g_3 \tag{35}$$

As mentioned before, if a_6 and a_8 are directly solved for from these two equations, there is a great chance that (a) although some data points will be matched exactly, the overall data fit will be of poor quality, and (b) the resulting yield surface will not be convex. Instead, to improve the chances of obtaining a good data fit and a convex yield surface, we will require that the above equations be satisfied in an average form at as many locations as possible. Thus, for $i = 1, 2$, we denote $c_i = \cos^2\theta_i$, $s_i = \sin^2\theta_i$, with $\theta_1 = 15°$, $\theta_2 = 75°$ (or $\theta_1 = 30°$, $\theta_2 = 60°$, or any combination of data on the corresponding intervals). Then we find a_6 and a_8 by optimizing the distance (or error) function

$$\psi := \frac{1}{2}\sum_{i=1,2}\left\{w_1^{(i)}[(c_i^2 - c_i s_i)a_6 + (s_i^2 - c_i s_i)a_8 - (B_6(\theta_i) - B_5 c_i s_i)]^2 . + w_2^{(i)}[(g_1(\theta_i) - g_3(\theta_i))a_6 + (g_2(\theta_i) - g_3(\theta_i))a_8 - (B_7(\theta_i) - B_5 g_3(\theta_i))]^2\right\} \tag{36}$$

where the weights $w_j^{(i)}$ are as follows: $w_1^{(i)}$ weights the data points $\bar{\sigma}_\theta$, whereas $w_2^{(i)}$ weights the data points r_θ at the locations θ_i. The optimization process is restricted to the rectangle $(a_6, a_8) \in [0, 6\sqrt{a_5 a_9}] \times [0, 6\sqrt{a_5 a_9}]$. The weights $w_j^{(i)}$ are kept fixed during minimization, but can be adjusted for each trial depending on the desired accuracy of the fit for each data point, and of the convexity of the yield surface.

The distance function ψ is a positive definite (assuming not all $w_j^{(i)}$ are zero) quadratic in a_6 and a_8, and therefore the solution to the minimization problem exists, is unique, and can be found in explicit form. After solving for a_6 and a_8 from the linear system $\partial\phi/\partial a_6 = 0$, $\partial\phi/\partial a_8 = 0$, the solution to the unrestricted minimization problem is

$$a_6 = \frac{k_{22} r_1 - k_{12} r_2}{k_{11} k_{22} - k_{12}^2}, \quad a_8 = \frac{k_{11} r_2 - k_{12} r_1}{k_{11} k_{22} - k_{12}^2} \tag{37}$$

where

$$k_{11} := \sum_{i=1,2} [w_1^{(i)} (\alpha_6^i)^2 + w_2^{(i)} (\beta_6^i)^2] \tag{38}$$

$$k_{22} := \sum_{i=1,2} [w_1^{(i)} (\alpha_8^i)^2 + w_2^{(i)} (\beta_8^i)^2] \tag{39}$$

$$k_{12} := \sum_{i=1,2} (w_1^{(i)} \alpha_6^i \alpha_8^i + w_2^{(i)} \beta_6^i \beta_8^i) \tag{40}$$

$$r_1 := \sum_{i=1,2} (w_1^{(i)} \alpha_6^i \alpha_0^i + w_2^{(i)} \beta_6^i \beta_0^i) \tag{41}$$

$$r_2 := \sum_{i=1,2} (w_1^{(i)} \alpha_8^i \alpha_0^i + w_2^{(i)} \beta_8^i \beta_0^i) \tag{42}$$

The α's and β's in the above formulas are the coefficients appearing in the expression of the distance function, Eq. (56):

$$\alpha_6^i := c_i^2 - c_i s_i, \quad \alpha_8^i := s_i^2 - c_i s_i, \quad \alpha_0^i := B_6 - B_5 c_i s_i \tag{43}$$

$$\beta_6^i := g_1 - g_3, \quad \beta_8^i := g_2 - g_3, \quad \beta_0^i := B_7 - B_5 g_3 \tag{44}$$

In general, the values of a_6 and a_8 for which the Poly4 yield surface is convex form a strict subset of the rectangle defined by inequalities (24). However, the weights $w_j^{(i)}$ in Eq. (56) can always be adjusted with only a few trials such that the minimum of the distance function ϕ is first within the rectangle (24) and then within the convexity domain. More rigorously, it can be shown that if all the other coefficients of Poly4 have been identified as above, then there is always a set of weights $w_j^{(i)}$ such that the remaining coefficients a_6 and a_8, when computed according to (37), will ensure a convex Poly4 yield surface.

In summary, the identification program for the coefficients of Poly4 takes as input the data $\bar{\sigma}_0, r_0, \bar{\sigma}_{90}, r_{90}, \bar{\sigma}_b, \bar{\sigma}_{45}, r_{45}$, and $\bar{\sigma}_\theta$ and r_θ for $\theta = 15°$ and $75°$ (or $\theta = 30°$ and $60°$), and proceeds as follows:

1. Compute the coefficients a_1, a_2, a_4 and a_5 according to Eqs. (11) and (12);
2. Check inequalities (16) and (20). If $\bar{\sigma}_b$ is outside the bounding intervals, then this data point should be adjusted accordingly. Then compute the coefficient a_3 using Eq. (13);
3. Check inequality (25). If r_{45} is outside the bounding interval, then this data point, or rather the $\bar{\sigma}_{45}$ data point, should be adjusted accordingly. Then compute the coefficient a_9 using Eq. (21);
4. Compute the coefficients a_6 and a_8 according to Eq. (37). The pair (a_6, a_8) should at minimum satisfy the inequalities (24). Convexity of the yield surface can be always achieved by properly adjusting the weights $w_j^{(i)}$;
5. Compute $a_7 = B_5 - (a_6 + a_8)$.

3.3. Applications: the modeling of two aluminum alloys and of a mild steel

We exemplify the outlined identification procedure for Poly4 with three applications: The modeling of aluminum alloys 2090-T3 and 2008-T4, and of the Numisheet'93 mild steel. For all of these materials experimental data are listed in Table 1.

Table 1
Experimental data for AA2090-T3, AA2008-T4 and NUM'93 mild steel

	$\bar{\sigma}_0$	$\bar{\sigma}_{15}$	$\bar{\sigma}_{30}$	$\bar{\sigma}_{45}$	$\bar{\sigma}_{60}$	$\bar{\sigma}_{75}$	$\bar{\sigma}_{90}$	$\bar{\sigma}_b$
2090-T3	1.0000	0.9605	0.9102	0.8114	0.8096	0.8815	0.9102	1.0350
2008-T4	1.0000	0.9963	0.9835	0.9459	0.9303	0.9171	0.9044	0.9010
NUM'93	1.0000	–	–	1.0569	–	–	1.0329	–
	r_0	r_{15}	r_{30}	r_{45}	r_{60}	r_{75}	r_{90}	r_b
2090-T3	0.2115	0.3269	0.6923	1.5769	1.0385	0.5384	0.6923	0.6700
2008-T4	0.8674	0.8077	0.6188	0.4915	0.4955	0.5114	0.5313	–
NUM'93	1.79	–	–	1.51	–	–	2.27	–

For AA2090-T3 inequalities (16) and (20) are satisfied in the form

$$0.8715 = 1/\bar{\sigma}_b^4 > 0.0435, \quad 0.6323 \leqslant \bar{\sigma}_b = 1.0350 \leqslant 1.0353 \tag{45}$$

It follows that P_4 can model the entire biaxial data set for this material with a real-valued convex yield curve. Next, inequality (25) is also satisfied in the form

$$0.5935 \leqslant r_{45} = 1.5769 \leqslant 20.169 \tag{46}$$

The bounding intervals for a_6 and a_8 are

$$0 \leqslant a_6 \leqslant 29.054, \quad 0 \leqslant a_8 \leqslant 35.068 \tag{47}$$

Then, due to the peculiar oscillation in r-value data around 75° from rolling, we use $\theta_1 = 15°$ and $\theta_2 = 75°$ as locations for the identification of a_6 and a_8. After a few minimization trials (with various weights starting with $w_1^{(1)} = 1.00, w_2^{(1)} = 1.00, w_1^{(2)} = 1.00, w_2^{(2)} = 1.00$), we find an acceptable material characterization listed in Table 2. The final weights used were: $w_1^{(1)} = 2.00, w_2^{(1)} = 1.00, w_1^{(2)} = 4.00, w_2^{(2)} = 0.30$ (recall that $w_1^{(i)}$ weighs $\bar{\sigma}_{\theta i}$, and $w_2^{(i)}$ weighs $r_{\theta i}$).

For AA2008-T4, inequalities (16), (20) and (25), are satisfied in the form $1.517 > 0.051$, $0.6428 \leqslant 0.9010 \leqslant 1.2230$, $0.1348 \leqslant 0.4915 \leqslant 5.5852$, respectively, whereas the bounding intervals for a_6 and a_8 are $0 \leqslant a_6 \leqslant 17.1410, 0 \leqslant a_8 \leqslant 20.9554$. Finally, using $\bar{\sigma}_\theta$ and r_θ at 15° and 75° from rolling for the identification of a_6 and a_8, we find the material characterization listed in Table 2 (the corresponding weights were $w_1^{(1)} = 2.00, w_2^{(1)} = 1.00, w_1^{(2)} = 0.10, w_2^{(2)} = 0.50$).

Results for the two alloys are presented in Figs. 1–3. Comparisons with Yld96 are also shown. Poly4 and Yld96 have different numbers of material coefficients for the description of the in plane plastic properties, nine and seven, respectively, but their modeling capabilities are of similar strength, with a slight advantage of Poly4, due to the explicit

Table 2
Poly4 coefficients for AA2090-T3, AA2008-T4 and NUM'93 mild steel

	a_1	a_2	a_3	a_4	a_5	a_6	a_7	a_8	a_9
2090-T3	1.0000	−0.6984	1.4969	−2.3838	1.4568	4.8808	−1.0150	8.7095	23.4498
2008-T4	1.0000	−1.8579	2.9549	−2.0742	1.4946	6.5600	−4.1447	7.9490	8.1031
NUM'93	1.0000	−2.5663	3.6988	−2.4392	0.8784	5.7851	−7.6630	5.8435	8.2863

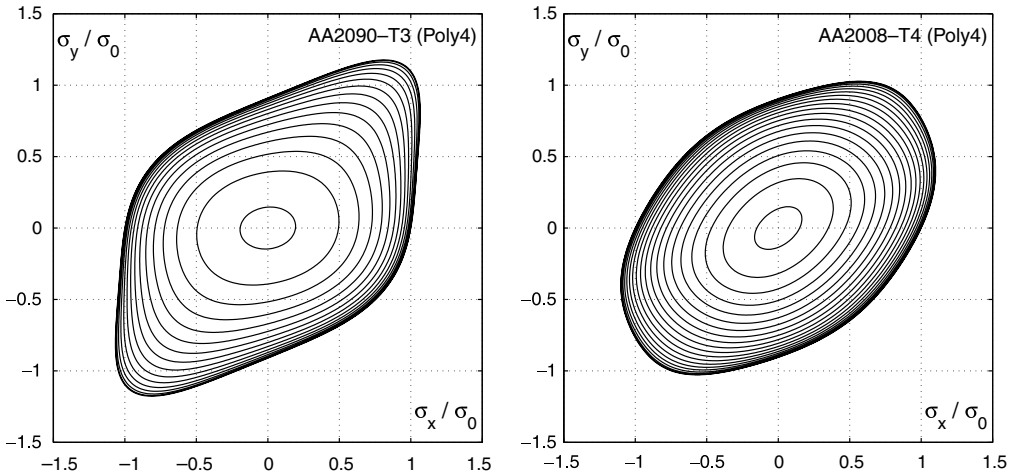

Fig. 1. Projections on the biaxial plane of the Poly4 yield surface for AA2090-T3 and AA2008-T4.

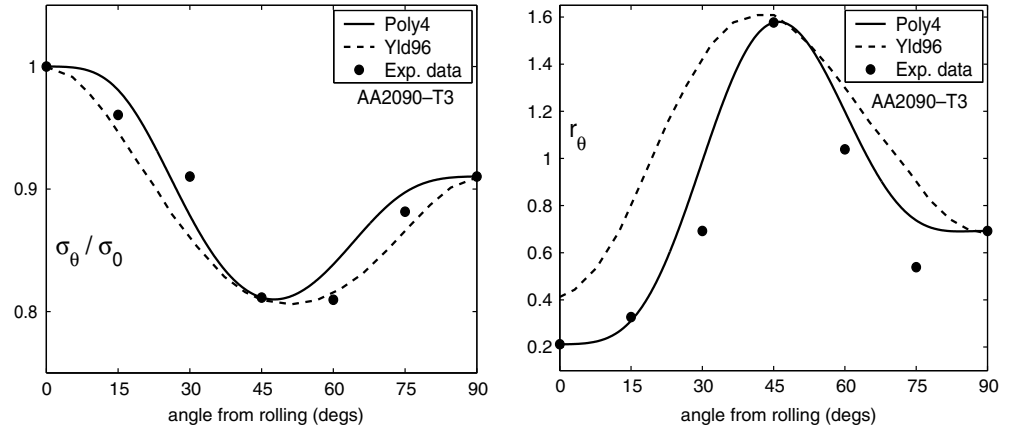

Fig. 2. Poly4 material characterization of AA2090-T3: directional yield strength (left) and *r*-value (right); comparison with Yld96 is also shown.

identification formulas and two extra parameters. Both criteria offer considerable improvement in modeling over Hill's quadratic criterion, by taking into account the directional variation of both the yield stress and *r*-value. However, it should be noted here that the two criteria are quite different at predicting the overall shape of the yield surface. While Poly4 yield surfaces are in general much more similar in shape with the quadratic yield surfaces (with their characteristic oval shape near equibiaxial stress state), Yld96 yield surfaces are in general much closer to the yield surface shapes predicted by Hosford type criteria, Hosford (1972). This aspect differentiates Poly4 and Yld96 with respect to the range of applications. For example, forming limit diagram predictions are known to be extremely sensitive to the shape of the biaxial yield curve. For this problem, in particular for aluminum alloys, Yld96 should be the first choice since it is specifically designed for better modeling of the biaxial yield curve, Barlat et al. (1997). On the other hand, Poly4 can be

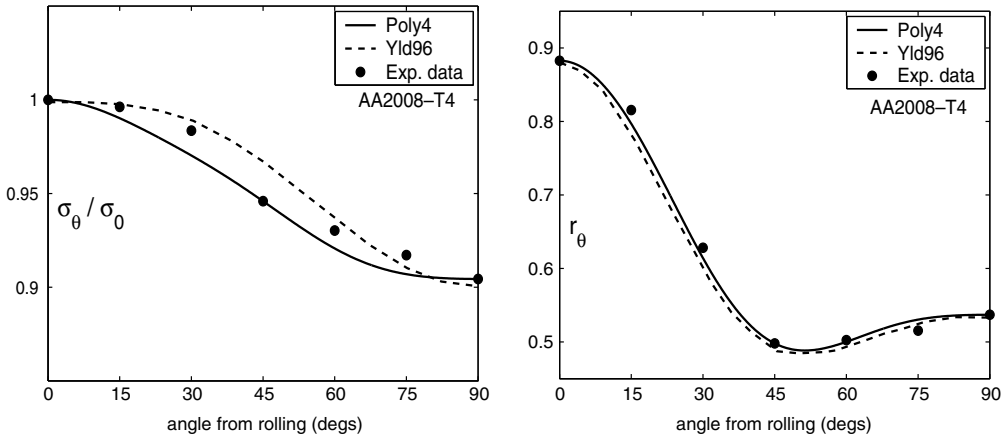

Fig. 3. Poly4 material characterization of AA2008-T4: Directional yield strength (left) and r-value (right); comparison with Yld96 is also shown.

easily used in any situation where Hill's quadratic is suitable, Poly4 offering an increased accuracy in material modeling.

It often happens that only three data points are available for yield strength, $\bar{\sigma}_0, \bar{\sigma}_{45}, \bar{\sigma}_{90}$, and only three data points for r-value, r_0, r_{45}, and r_{90}, with no indication about the value of the biaxial yield strength. This is the case with the Numisheet'93 mild steel, Danckert (1995), referred from now on as NUM93. Poly4 can still be applied to the modeling of such data sets as follows. First, the biaxial yield strength is postulated for this material to be $\bar{\sigma}_b = 1.15$ (the bounds for this data point are $0.7956 \leqslant \bar{\sigma}_b \leqslant 1.9587$). This is in agreement with data for a similar steel studied in Pearce (1968). Then, the intermediary data can be estimated according to the formulas

$$\bar{\sigma}_{\theta_1} = \alpha_1 \bar{\sigma}_0 + \beta_1 \bar{\sigma}_{45}, \quad \bar{\sigma}_{\theta_2} = \alpha_2 \bar{\sigma}_{45} + \beta_2 \bar{\sigma}_{90}, \quad \alpha_i + \beta_i = 1 \tag{48}$$

$$r_{\theta_1} = \gamma_1 r_0 + \delta_1 r_{45}, \quad r_{\theta_2} = \gamma_2 r_{45} + \delta_2 r_{90}, \quad \gamma_i + \delta_i = 1 \tag{49}$$

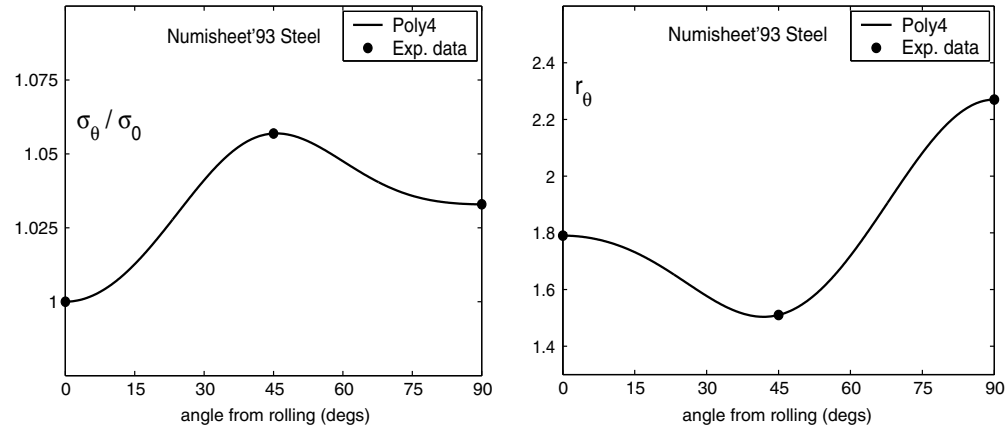

Fig. 4. Poly4 material characterization of the NUM'93 mild steel: Directional yield strength (left) and r-value (right).

For NUM93 we use $\theta_1 = 30°$, and $\theta_2 = 60°$. Then with $\alpha_1 = 0.3$, $\alpha_2 = 0.4$, $\gamma_1 = 0.2$, $\gamma_2 = 0.7$, and the weights $w_1^1 = 1.00, w_2^1 = 0.50, w_1^2 = 1.00$, and $w_2^2 = 0.10$, we obtain the coefficients listed in Table 2, and the results presented in Fig. 4.

4. Sixth and eighth-order polynomials (plane stress)

Although Poly4 offers increased modeling power when compared with Hill's quadratic polynomial, it still cannot achieve a completely satisfactorily description for materials such as AA2090-T3. In this section we explore higher order polynomials: of order six and eight. Thus, the yield function, for plane stress, is in the form of Eq. (7), with $n = 6$ or $n = 8$, and with the corresponding orthotropic polynomials

$$\begin{aligned} P_6 = {} & a_1\sigma_x^6 + a_2\sigma_x^5\sigma_y + a_3\sigma_x^4\sigma_y^2 + a_4\sigma_x^3\sigma_y^3 + a_5\sigma_x^2\sigma_y^4 + a_6\sigma_x\sigma_y^5 + a_7\sigma_y^6 + (a_8\sigma_x^4 \\ & + a_9\sigma_x^3\sigma_y + a_{10}\sigma_x^2\sigma_y^2 + a_{11}\sigma_x\sigma_y^3 + a_{12}\sigma_y^4)\sigma_{xy}^2 + (a_{13}\sigma_x^2 + a_{14}\sigma_x\sigma_y + a_{15}\sigma_y^2)\sigma_{xy}^4 \\ & + a_{16}\sigma_{xy}^6 \end{aligned} \tag{50}$$

$$\begin{aligned} P_8 = {} & a_1\sigma_x^8 + a_2\sigma_x^7\sigma_y + a_3\sigma_x^6\sigma_y^2 + a_4\sigma_x^5\sigma_y^3 + a_5\sigma_x^4\sigma_y^4 + a_6\sigma_x^3\sigma_y^5 + a_7\sigma_x^2\sigma_y^6 + a_8\sigma_x\sigma_y^7 \\ & + a_9\sigma_y^8 + (a_{10}\sigma_x^6 + a_{11}\sigma_x^5\sigma_y + a_{12}\sigma_x^4\sigma_y^2 + a_{13}\sigma_x^3\sigma_y^3 + a_{14}\sigma_x^2\sigma_y^4 + a_{15}\sigma_x\sigma_y^5 \\ & + a_{16}\sigma_y^6)\sigma_{xy}^2 + (a_{17}\sigma_x^4 + a_{18}\sigma_x^3\sigma_y + a_{19}\sigma_x^2\sigma_y^2 + a_{20}\sigma_x\sigma_y^3 + a_{21}\sigma_y^4)\sigma_{xy}^4 + (a_{22}\sigma_x^2 \\ & + a_{23}\sigma_x\sigma_y + a_{24}\sigma_y^2)\sigma_{xy}^6 + a_{25}\sigma_{xy}^8 \end{aligned} \tag{51}$$

For $n = 6$, the criterion in (7) will be referred to as Poly6, whereas for $n = 8$ it will be referred as Poly8. Poly6 and Poly8 have 16 and 25 material coefficients, respectively, for the description of the in-plane plastic properties. Thus, an analysis comparable with the one for Poly4 is no longer possible. Instead, we propose here a numerical approach for coefficient identification: the coefficients of Poly6 and Poly8 will be determined by minimizing the distance between predicted directional yield strengths and r-values, and the corresponding experimental data. To insure that the resulting yield surfaces are real-valued and convex, the optimization process will be subjected to positivity and convexity constraints. Constrained optimization subroutines are nowadays widely available. For the implementation of Poly6 and Poly8 we used the IMSL (D)N0ONF (or DNCONG) subroutine, which is a Fortran implementation of Schitkowski (1986). Such subroutines require the evaluation of the merit function, constraints and of their gradients. Although the algebra may seem a little tedious, it is on the other hand quite straightforward and we shall sketch it here rather than into an appendix. The reason is dual. First, the algorithm is general enough to be used with any other yield function, or with any other polynomial type strain-rate potential. Second, as we shall soon see at the end of this section and the ones dedicated to earing, Poly6 and Poly8 turn out to be powerful yield criteria, capable of modeling a wide range of anisotropic variations in plastic properties, and therefore some detail of their algorithmic implementation is worthwhile pursuing.

If σ_0 is chosen as reference yield strength (for isotropic hardening), the nth order polynomial P_n will then predict for a uniaxial test along an angle θ from the rolling direction

$$\sigma_0^n = \sigma_\theta^n P_n(\cos^2\theta, \sin^2\theta, \cos\theta\sin\theta) = \sigma_\theta^n Q(a_i, \theta) \Rightarrow \frac{1}{\bar{\sigma}_\theta^n} = Q(a_i, \theta) \tag{52}$$

The predicted r-value is computed according to the formula

$$r_\theta = \left[\frac{\partial P_n}{\partial \sigma_{xy}}\sin\theta\cos\theta - \left(\frac{\partial P_n}{\partial \sigma_x}\sin^2\theta + \frac{\partial P_n}{\partial \sigma_y}\cos^2\theta\right)\right] \Big/ \left(\frac{\partial P_n}{\partial \sigma_x} + \frac{\partial P_n}{\partial \sigma_y}\right)$$
$$= R_1(a_i,\theta)/R_2(a_i,\theta) \tag{53}$$

Similarly, the biaxial predictions, when $\sigma_x = \sigma_y = \sigma_b$, $\sigma_{xy} = 0$, are as follows

$$\sigma_0^n = \sigma_b^n P_n(1,1,0) = \sigma_b^n Q_b(a_i) \Rightarrow \frac{1}{\bar\sigma_b^n} = Q_b(a_i) \tag{54}$$

$$r_b := \frac{\partial f}{\partial \sigma_x}(\sigma_b,\sigma_b,0) \Big/ \frac{\partial f}{\partial \sigma_y}(\sigma_b,\sigma_b,0) = \frac{\partial P_n}{\partial \sigma_x}(1,1,0) \Big/ \frac{\partial P_n}{\partial \sigma_y}(1,1,0)$$
$$= R_{b1}(a_i)/R_{b2}(a_i) \tag{55}$$

The identification of the material coefficients is then performed by minimizing the distance function

$$g(a_i) = \frac{1}{2}\sum_{\theta_j}\left\{w_j^s[Q(a_i,\theta_j) - (\bar\sigma_{\theta_j})^{-n}]^2 + w_j^r[R_1(a_i,\theta_j) - r_{\theta_j}R_2(a_i,\theta_j)]^2\right\}$$
$$+ (1/2)\left\{w^{sb}[Q^b(a_i) - (\bar\sigma_b)^{-n}]^2 + w^{rb}[R_1^b(a_i) - r_b R_2^b(a_i)]^2\right\} \tag{56}$$

where w_j^s, w_j^r, w^{sb} and w^{rb} are weights associated with each data point. It should be noted that in (56), $\bar\sigma_{\theta j}, r_{\theta j}, \bar\sigma_b$, and r_b denote experimental data points, whereas $\bar\sigma_\theta, r_\theta, \bar\sigma_b$, and r_b in (52)–(54), and (55), respectively, denote predicted values. The gradient of the merit function (56) is

$$\frac{\partial g}{\partial a_k} = \sum_{\theta_j}\left\{w_j^s[Q(a_i,\theta_j) - (\bar\sigma_{\theta_j})^{-n}]\frac{\partial Q}{\partial a_k} + w_j^r[R_1(a_i,\theta_j) - r_{\theta_j}R_2(a_i,\theta_j)]\left(\frac{\partial R_1}{\partial a_k} - r_j\frac{\partial R_2}{\partial a_k}\right)\right\}$$
$$+ w^{sb}[Q_b(a_i) - (\bar\sigma_b)^{-n}]\frac{\partial Q_b}{\partial a_k} + w^{rb}[R_{b1}(a_i) - r_b R_{b2}(a_i)]\left(\frac{\partial R_{b1}}{\partial a_k} - r_{\theta_j}\frac{\partial R_{b2}}{\partial a_k}\right) \tag{57}$$

It is recalled that, due to the homogeneity of the polynomial functions involved, in the above formulas the quantities Q, R_1, R_2, and their derivatives are evaluated at ($\cos^2\theta$, -$\sin^2\theta$,cos $\theta\sin\theta$), as in (52), for example.

The optimization process is subjected to the constrains (9) to be implemented as follows. On the unit sphere $\sigma_x^2 + \sigma_y^2 + \sigma_{xy}^2 = 1$ we consider two families of unit circles. The first family is formed with constant longitude (vertical) circles parameterized in the form

$$\sigma_x = \cos\omega\cos\theta, \quad \sigma_y = \cos\omega\sin\theta, \quad \sigma_{xy} = \sin\omega, \quad \theta\in[0,\pi), \quad \omega\in[0,\pi) \tag{58}$$

Above we have $\omega \in [0, \pi)$ due to the orthotropic symmetry of the yield function (the yield surface in the space σ_x, σ_y, σ_{xy} is symmetric with respect to the $\sigma_{xy} = 0$ plane). Then impose the two inequality constraints (9) at discrete locations on each (semi)circle of the family. Thus, we consider $N^{(v)}$ vertical circles, described by $\theta_q = (q-1)\pi/N^{(v)}$, $q = 1, \ldots, N^{(v)}$, and on each such vertical circle we take $M^{(v)}$ points

$$\sigma_x^{qi} = \cos\omega_i\cos\theta_q, \quad \sigma_y^{qi} = \cos\omega_i\sin\theta_q, \quad \sigma_{xy} = \sin\omega_i,$$
$$\omega_i = (i-1)\pi/M^{(v)}, \quad i = 1,\ldots,M^{(v)} \tag{59}$$

For each such point we then have the constraints

$$g^p_{qi}(a_j) := P_n(\sigma_x^{qi}, \sigma_y^{qi}, \sigma_{xy}^{qi}) > 0 \tag{60}$$

$$g^c_{qi}(a_j) := n^2[P_n(\sigma_x^{qi}, \sigma_y^{qi}, \sigma_{xy}^{qi})]^2 - (n-1)[P'_n(\sigma_x^{qi}, \sigma_y^{qi}, \sigma_{xy}^{qi})]^2 + nP_n(\sigma_x^{qi}, \sigma_y^{qi}, \sigma_{xy}^{qi})P''_n(\sigma_x^{qi}, \sigma_y^{qi}, \sigma_{xy}^{qi}) \geqslant 0 \tag{61}$$

The second family is formed with constant latitude (horizontal) circles parameterized in the form

$$\sigma_x = \cos\omega \sin\theta, \quad \sigma_y = \sin\omega \sin\theta, \quad \sigma_{xy} = \cos\theta, \quad \theta \in [0, \frac{\pi}{2}), \quad \omega \in [0, \pi) \tag{62}$$

Above we have $\theta \in [0, \pi/2)$ due to the orthotropic symmetry, and $\omega \in [0, \pi)$ due to the central symmetry of the yield surface. Again, we consider $N^{(h)}$ horizontal circles, described by $\theta_q = (q-1)\pi/(2N^{(h)})$, $q = 1, \ldots, N^{(h)}$, and on each such horizontal circle we take $M^{(h)}$ points

$$\sigma_x^{qi} = \cos\omega_i \sin\theta_q, \quad \sigma_y^{qi} = \sin\omega_i \sin\theta_q, \quad \sigma_{xy}^{q} = \cos\theta_q,$$
$$\omega_i = (i-1)\pi/M^{(h)}, \quad i = 1, \ldots, M^{(h)} \tag{63}$$

At each such point we then write again the constraints (60) and (61).

Finally, one needs to specify the gradients of the constraints. For the positivity constraints (60) this is a trivial task since P_n depends linearly on its coefficients a_k. The gradients of the convexity constraints (61) are also easily implemented by noting that

$$P'_n = \frac{\mathrm{d}}{\mathrm{d}\omega} P_n(\sigma_x, \sigma_y, \sigma_{xy}) = \nabla P_n \cdot V \tag{64}$$

$$P''_n = \frac{\mathrm{d}^2}{\mathrm{d}\omega^2} P_n(\sigma_x, \sigma_y, \sigma_{xy}) = (\nabla^2 P_n \cdot V) \cdot V + \nabla P_n \cdot A \tag{65}$$

where

$$\nabla P_n = \left[\frac{\partial P_n}{\partial \sigma_x}, \frac{\partial P_n}{\partial \sigma_y}, \frac{\partial P_n}{\partial \sigma_{xy}}\right], \quad \nabla^2 P_n = \begin{bmatrix} \frac{\partial^2 P_n}{\partial \sigma_x \partial \sigma_x} & \frac{\partial^2 P_n}{\partial \sigma_x \partial \sigma_y} & \frac{\partial^2 P_n}{\partial \sigma_x \partial \sigma_{xy}} \\ \frac{\partial^2 P_n}{\partial \sigma_x \partial \sigma_y} & \frac{\partial^2 P_n}{\partial \sigma_y \partial \sigma_y} & \frac{\partial^2 P_n}{\partial \sigma_y \partial \sigma_{xy}} \\ \frac{\partial^2 P_n}{\partial \sigma_x \partial \sigma_{xy}} & \frac{\partial^2 P_n}{\partial \sigma_y \partial \sigma_{xy}} & \frac{\partial^2 P_n}{\partial \sigma_{xy} \partial \sigma_{xy}} \end{bmatrix}, \tag{66}$$

$$V = \frac{\mathrm{d}}{\mathrm{d}\omega}[\sigma_x, \sigma_y, \sigma_{xy}]^{\mathrm{T}}, \quad A = \frac{\mathrm{d}^2}{\mathrm{d}\omega^2}[\sigma_x, \sigma_y, \sigma_{xy}]^{\mathrm{T}}, \tag{67}$$

where $[\sigma_x, \sigma_y, \sigma_{xy}]$ is parameterized by (58) or (62). Thus, the task of writing the gradient of (61) is reduced to computing the gradients with respect to a_k of P_n, its first and second derivatives.

In practice, for Poly6 it is enough to take $4 \leqslant N^{(v)} \leqslant 8$, $10 \leqslant M^{(v)} \leqslant 20$,$1 \leqslant N^{(h)} \leqslant 4$, and $10 \leqslant M^{(h)} \leqslant 20$, so that the identified yield surface is real-valued and convex. For Poly8 one may take $20 \leqslant N^{(v)} \leqslant 40$, $10 \leqslant M^{(v)} \leqslant 20$, $2 \leqslant N^{(h)} \leqslant 4$, and $10 \leqslant M^{(h)} \leqslant 20$.

The coefficient a_1 can be taken as 1.000 from the beginning, the optimization being done on the rest of the coefficients. As initial guesses, $a_k^{(0)}$, for Poly6 and Poly8 one can

always use the coefficients of the isotropic von Mises criterion. That is, if I denotes the isotropic quadratic criterion of von Mises, then the isotropic Poly6 and Poly8 are found from $P_n = I^{n/2}$. The isotropic coefficients for Poly6 and Poly8 are provided in Tables 3 and 4. An alternative initial guess for Poly8 is the coefficient vector provided by Poly4. The connection between the two sets of coefficients is listed in Appendix 2. Then, the constrained optimization problem is solved within the hypercube

$$\prod_{k=1}^{N}[a_k^{(0)} - b, a_k^{(0)} + b],$$

where N being the number of coefficients, and where b should be in general chosen as a small quantity in order to avoid "slipping" of the solution, e.g., $0 < b < 10$.

The solution to the first problem is then taken as initial guess to the same optimization problem, and so on, the process being stopped when the desired accuracy has been met.

The identification program described in this section has been applied to the modeling of AA2090-T3. The coefficients of Poly6 and Poly8 for this material are listed in Tables 3 and 4. The corresponding real-valued and convex yield surfaces are plotted in Fig. 5. The predictions of Poly6 and Poly8 for directional yield strength and r-value are presented in Fig. 6, where comparisons with Yld2004 are also made. Besides these results, Poly6 predictions for biaxial yield strength and biaxial r-value are 1.033 and 0.668, respectively,

Table 3
Poly6 coefficients for isotropic Mises, AA2090-T3, Mat_1, and Mat_2

	a_1	a_2	a_3	a_4	a_5	a_6	a_7	a_8
Mises	1.0	−3.0	6.0	−7.0	6.0	−3.0	1.0	9.0
2090T3	1.0000	−1.1059	2.5255	−5.1914	6.1458	−4.3254	1.7753	14.190
Mat_1	1.0000	−1.1880	3.0973	−5.3635	4.8054	−2.3524	1.0033	7.0845
Mat_2	1.0000	−2.9990	4.6492	−5.1746	6.7131	−5.0622	1.6875	12.992
	a_9	a_{10}	a_{11}	a_{12}	a_{13}	a_{14}	a_{15}	a_{16}
Mises	−18.0	27.0	−18.0	9.0	27.0	27.0	27.0	27.0
2090T3	−4.9759	−4.3926	3.4652	15.806	0.0000	−9.4916	86.661	116.42
Mat_1	−4.5822	12.961	−7.1405	8.2028	17.488	−35.292	18.514	45.591
Mat_2	−19.385	22.582	−42.882	34.406	42.562	−17.915	100.67	57.077

Table 4
Poly8 coefficients for isotropic Mises and AA2090-T3

	a_2	a_3	a_4	a_5	a_6	a_7	a_8	a_9
Mises	−4	10	−16	19	−16	10	−4	1
2090T3	−1.3376	2.1967	−5.7867	12.312	−16.000	13.260	−7.0415	2.1508
	a_{10}	a_{11}	a_{12}	a_{13}	a_{14}	a_{15}	a_{16}	a_{17}
Mises	12	−36	72	−84	72	−36	12	54
2090T3	12.697	−4.2719	74.294	−31.487	−18.387	−11.096	28.553	116.65
	a_{18}	a_{19}	a_{20}	a_{21}	a_{22}	a_{23}	a_{24}	a_{25}
Mises	−108	162	−108	54	108	−108	108	81
2090T3	−238.83	158.71	−57.545	172.28	−0.2559	−8.2036	558.15	543.50

For both we have $a_1 = 1.0000$.

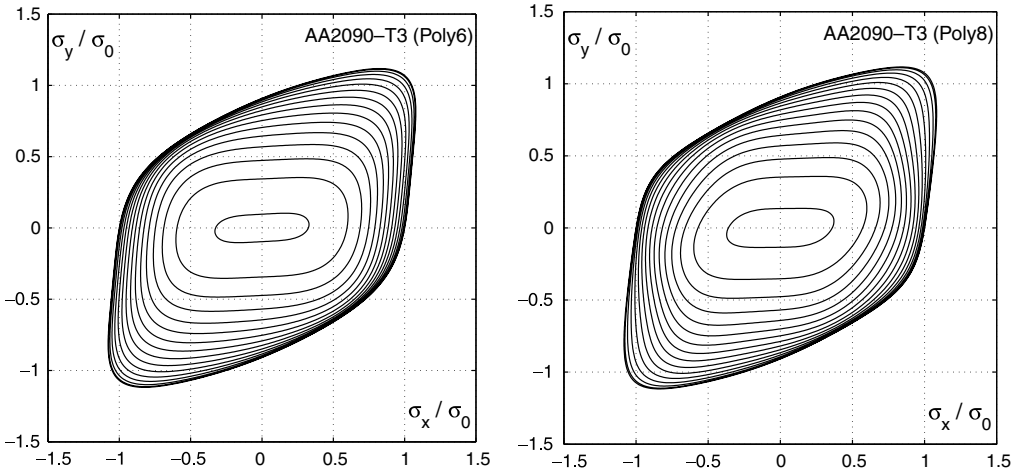

Fig. 5. Projections on the biaxial plane of the Poly6 (left) and Poly8 (right) yield surfaces for AA2090-T3.

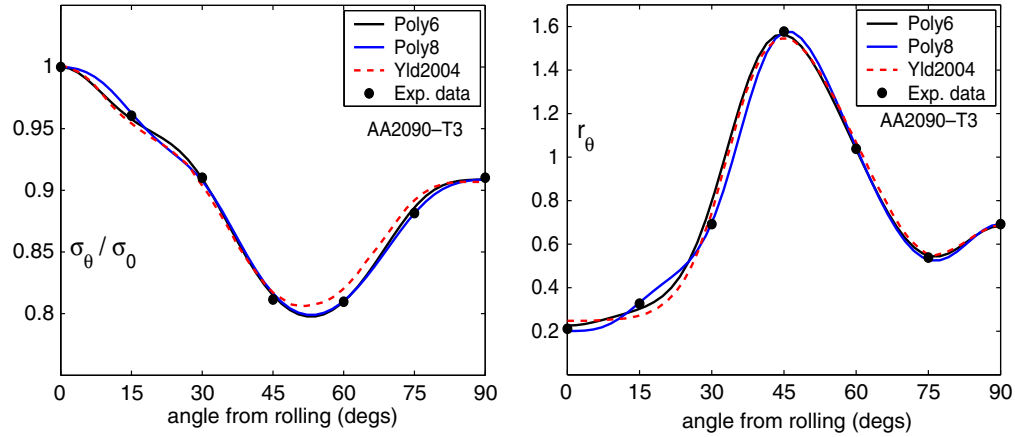

Fig. 6. Poly6 and Poly8 material characterization of AA2090-T3: directional yield strength (left) and r-value (right); comparison with Yld2004 is also shown.

whereas the biaxial Poly8 predictions are 1.036 and 0.670, respectively. From these results we conclude that Poly6 and Poly8 give perfect solutions to the characterization of this alloy. Further applications of Poly6 are presented in the following sections.

5. Extensions to 3D stress states

Polynomial yield functions for 3D stress states can be built up as for the case of plane stress, with a small additional precaution since here the pressure independence condition has to be taken care of. First, we notice that from Eqs. (2) and (3), it follows that any orthotropic polynomial yield function for 3D stress states must depend on the shear components σ_{xy}, σ_{xz} and σ_{yz} only through the monomials

$$\sigma_{xy}^2, \quad \sigma_{xz}^2, \quad \sigma_{yz}^2, \quad \sigma_{xy}\sigma_{xz}\sigma_{yz} \tag{68}$$

Then, in order to satisfy the pressure independence condition, one can consider as yield function a general nth-order polynomial of the stress components s_x, s_y, s_z, s_{xy}, s_{xz}, s_{yz} of the deviatoric stress tensor, $s = \sigma - [(\sigma_x + \sigma_y + \sigma_z)/3]\mathbf{I}$. However, taking into account that $s_z = -(s_x + s_y)$, it is enough to consider polynomial expressions in the five variables s_x, s_y, s_{xy}, s_{xz}, s_{yz}. Finally, since $s_{xy} = \sigma_{xy}$, $s_{xz} = \sigma_{xz}$, $s_{yz} = \sigma_{yz}$, the orthotropic symmetry of the criterion is satisfied if we eliminate from the polynomial those monomials that contain products of the form $\sigma_{xy}^i \alpha_{xz}^j \sigma_{yz}^k$, where i, j, and k are not all even, or do not respect the equality $i = j = k$. For example, a 3D pressure independent and orthotropic fourth-order polynomial will have the expression

$$\begin{aligned} P_4^{(3D)} = {} & a_1 s_x^4 + a_2 s_x^3 s_y + a_3 s_x^2 s_y^2 + a_4 s_x s_y^3 + a_5 s_y^4 + (a_6 s_x^2 + a_7 s_x s_y + a_8 s_y^2)\sigma_{xy}^2 \\ & + (a_9 s_x^2 + a_{10} s_x s_y + a_{11} s_y^2)\sigma_{xz}^2 + (a_{12} s_x^2 + a_{13} s_x s_y + a_{14} s_y^2)\sigma_{yz}^2 \\ & + (a_{15} s_x + a_{16} s_y)\sigma_{xy}\sigma_{xz}\sigma_{yz} + a_{17}\sigma_{xy}^2\sigma_{xz}^2 + a_{18}\sigma_{xy}^2\sigma_{yz}^2 + a_{19}\sigma_{xz}^2\sigma_{yz}^2 \\ & + a_{20}\sigma_{xy}^4 + a_{21}\sigma_{xz}^4 + a_{22}\sigma_{yz}^4 \end{aligned} \tag{69}$$

This approach has been considered before by Arminjon et al. (1994), to build strain rate potentials. They also double checked their polynomial form, for the correct number of coefficients, with a polynomial construction based on generalized (anisotropic) invariants. A similar 3D polynomial criterion can be easily built from a sixth-order homogeneous polynomial and so on. However, since the number of coefficients increases rapidly with the degree of homogeneity, the usefulness of such 3D criteria becomes doubtful in the absence of a sufficient number of out of plane experimental data points. An alternative is to use polynomial criteria as strain rate potentials and to associate the coefficients with texture information, e.g., Arminjon et al. (1994), Zhou et al. (1998). Yet again, the issue of convexity must be dealt with during the identification phase even for this approach. The general method described in the previous section is applicable in this case too, with fewer constraints being needed for this type of potential, due to the large amount of data.

When the identification of the yield function is based on yield and flow data obtained from mechanical tests, the above approach is clearly unsuited, since out of plane data is scarcely available for thin metallic sheets, therefore leaving undetermined most of the coefficients related to the out of plane shears σ_{xz} and σ_{yz}. A simpler methodology is possible for directly extending plane stress criteria to 3D stress states while keeping the number of additional coefficients to a minimum. First, the pressure independence condition is satisfied by a yield function f if and only if

$$f(\boldsymbol{\sigma}) = f(\sigma_x - \sigma_z, \sigma_y - \sigma_z, \sigma_{xy}, \sigma_{xz}, \sigma_{yz}) \tag{70}$$

Indeed, the subspace of deviatoric stresses, denote it V', can be written as a direct product between the two-dimensional subspace Π defined by $\sigma_x + \sigma_y + \sigma_z = 0$, and the subspace of the shear components $S := \{(\sigma_{xy}, \sigma_{xz}, \sigma_{yz}) \in \mathbb{R}^3\}$,

$$V' = \Pi \times S \tag{71}$$

A pressure independent yield function f is then uniquely determined by its restriction to V'. Eq. (70) then follows immediately if we observe that the Π plane can be parameterized in the form

$$\sigma_x = (2s_1 - s_2)/3, \quad \sigma_y = (-s_1 + 2s_2)/3, \quad \sigma_z = -(s_1 + s_2)/3 \tag{72}$$

where $s_1 := \sigma_x - \sigma_z$, and $s_2 := \sigma_y - \sigma_z$. As a consequence, in Eq. (69) one may also replace the the deviatoric components with $s_x := s_1$, and $\sigma_y := s_2$. Let us next denote

$$g(\sigma_x, \sigma_y, \sigma_z, \sigma_{xy}) := f(\sigma_x - \sigma_z, \sigma_y - \sigma_z, \sigma_{xy}, 0, 0) \tag{73}$$

as that part of the 3D criterion which contains the coupling between the plane stress state and the normal component. On the other hand, the plane stress restriction of the 3D criterion is

$$f^{(2D)}(\sigma_x, \sigma_y, \sigma_{xy}) = f(\sigma_x, \sigma_y, \sigma_{xy}, 0, 0) \tag{74}$$

Therefore one can completely recuperate the 3D part g from f, from the 2D (plane stress) criterion by a simple linear transformation

$$g(\sigma_x, \sigma_y, \sigma_z, \sigma_{xy}) = f^{(2D)}(\sigma_x - \sigma_z, \sigma_y - \sigma_z, \sigma_{xy}) \tag{75}$$

To complete the 3D formulation of the yield function from its plane stress restriction, one only needs to add the out of plane shear coupling with the plane stress and normal components. This extension can be designed depending on how many out of plane data points are available. For example, we propose the following minimalist 3D extension of plane stress yield functions given by Eq. (7):

$$\bar{\sigma}^2 = [P_n^{(2D)}(\sigma_x - \sigma_z, \sigma_y - \sigma_z, \sigma_{xy})]^{2/n} + 2k_{13}\sigma_{xz}^2 + 2k_{23}\sigma_{yz}^2 \tag{76}$$

First, we note that this extension can be reduced to Hill'48 (or Mises) criterion. Second, once the plane stress restriction is convex, the above 3D extension is also convex. Indeed, the 3D extension is in the form $f(\boldsymbol{\sigma}) = \{[f_1(\boldsymbol{\sigma})]^2 + [f_2(\boldsymbol{\sigma})]^2\}^{1/2}$, and the function f will be convex if f_1 and f_2 are positive convex functions. In our case, f_2 is always in the form $f_2(\boldsymbol{\sigma}) = [2k_{13}\sigma_{xz}^2 + 2k_{23}\sigma_{yz}^2]^{1/2}$, with k_{13} and k_{23} positive coefficients. Thus f_2 is positive and convex. On the other hand, f_1 is obtained by a linear transformation from the 2D restriction: $f_1(\boldsymbol{\sigma}) = [P_n^{(2D)}(\sigma_x - \sigma_z, \sigma_y - \sigma_z, \sigma_{xy})]^{1/n}$, and therefore f_1 will be positive and convex if $(P_n^{(2D)})^{1/n}$ is positive and convex.

6. Applications to deep drawing

The polynomial approach to developing anisotropic yield functions reduces the implementation of such functions into finite element (FE) codes to an almost trivial task. Once the integration scheme for the constitutive model has been agreed upon, the only input left for specification is the evaluation of the yield function, its gradient and, possibly, its Hessian, which are all routine calculations for polynomial functions. This section presents results from the FE simulations of two deep drawing processes: The forming of square and cylindrical cups. For this purpose we used the commercial FE code ABAQUS (Standard) in which we implemented the Poly4, Poly6 and Poly8 plane stress and 3D yield functions as UMAT subroutines. The algorithm used for the integration of the constitutive equations was based on the fully implicit backward Euler scheme, also known as the return mapping algorithm. For more details on this matter the reader is referred to the excellent book of Simo and Hughes (1999), or to the work of Tuğcu and Neale (1999) for example.

6.1. The Numisheet'93 square cup test

The Numisheet'93 square cup problem is solved using plane stress Poly4 yield function. It was proposed by the Numisheet committee as a benchmark for FE codes. The goal is to

predict the correct deformed shape of the square cup at several locations during punch travel, as well as the correct distribution of the thickness strain within the deformed sheet. Predicting the correct strain distribution in the cup is essential for this problem, since near the corners of the punch the sheet is prone to failure (necking/fracture in plane strain conditions), the correct strain distribution prediction leading to a correct design of the process.

The geometrical setting of the problem in the XZ-plane is similar with the one for the deep drawing of cylindrical cups, to be discussed in the next section, and is depicted in Fig. 9. In the XZ-plane the shoulder of the punch has a radius of 8 mm, whereas the shoulder of the die has a radius of 5 mm. The difference is in the shape of the tools in the XY-plane which is circular for the cylindrical case, and square for this problem, depicted in Fig. 7. The blank is a $150 \times 150 \times 0.78$ mm sheet, made from NUM'93 mild steel modeled in Section 3.3, with Poly4 coefficients listed in Table 2. The other parameters of the simulation were given as follows, Danckert (1995):

- Isotropic elasticity: $E = 206$ GPa, $v = 0.3$,
- Isotropic hardening curve: $\bar{\sigma} = 565.32(0.007117 + \bar{\epsilon})^{0.2589}$ MPa,
- Coulomb coefficient of friction: 0.144,
- Blank holding force: 19.6 kN (4.9 kN for a quarter region).

Considering the geometrical and material symmetry of the problem, only a quarter of the entire geometry was simulated. The quarter blank was meshed with 20×20 SC8R shell elements (15 integration points across the thickness), whereas the tools were meshed as discrete rigid parts. In Fig. 7 the profile of the final drawn cup (at 40 mm punch travel) is shown, whereas Table 5 lists the amount of draw-in at 15 and 40 mm punch travel. As can be seen, the amount of draw-in predicted by the Poly4 simulation agrees very well with the experimentally measured data. A comparison analysis with the blank considered

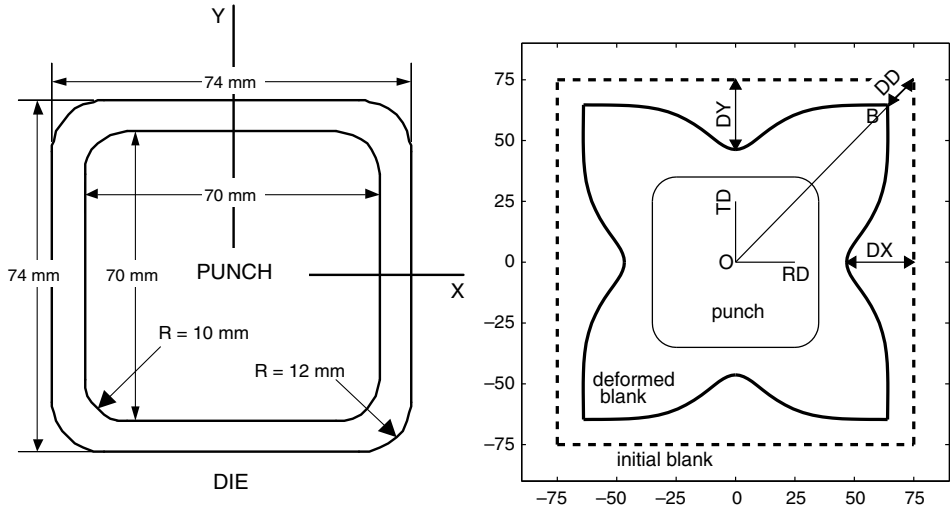

Fig. 7. Tool dimensions for the square cup problem (left) and profile of the drawn cup (at 40 mm punch stroke) with definitions of draw-in (right - dimensions in mm).

Table 5
Draw-in predictions of Poly4 FE simulation and experimental data

Punch travel (mm)	DX (mm)		DY (mm)		DD (mm)	
	FE	Exp.	FE	Exp.	FE	Exp.
15	5.94	5.64	6.06	6.63	3.28	3.48
40	28.24	27.89	28.68	29.24	15.10	15.95

plastically isotropic, and modeled with (ABAQUS) von Mises criterion, was also conducted. The final profile, and thus the amount of draw-in in all three directions, predicted by the isotropic analysis was virtually identical with the one predicted by the Poly4 analysis. Thus, the plastic anisotropy of the sheet has very little or at all influence on the final shape of the profile, and this is due to the initial square shape of the blank which inhibits the development of such effects (see also the discussion on earing, next). However, the strain distributions predicted by the two analyzes differ. Fig. 8 shows the thickness strains predicted by the two simulations along the *OB* diagonal of the blank, see Fig. 5, and we conclude that the Poly4 simulation has better agreement with the experimental data than the isotropic (von Mises) simulation. This is an effect of the plastic anisotropy of the sheet.

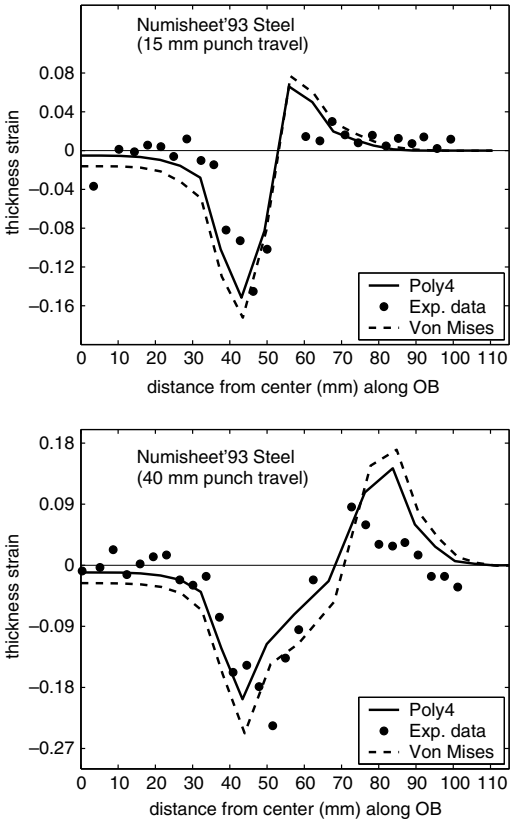

Fig. 8. Thickness strain variation along the OB diagonal as predicted by FE simulations with Poly4 and Von Mises, and as measured at 15 mm and 40 mm punch strokes.

6.2. Prediction of earing in cylindrical cups

The deep drawing of cylindrical cups from metallic sheets is one of the forming operations where the effects of the yielding anisotropy are most evident. For an anisotropic sheet, the height (profile) of the drawn cup is not uniform (as in the case of an isotropic material), but shows a series of maxima and minima commonly known as ears and troughs (hollows). Depending on how strong this anisotropy is, the profile can have four, six, etc, ears. Boundary conditions of loading process, e.g., friction, holding force, etc, also have an important effect on the magnitude of the ears. The objective of this benchmark is to predict the correct number of ears and the height of the cup's profile.

For the AA2090-T3 sheet, the geometrical setting and specific tool dimensions are taken from Yoon et al. (2000), see Fig. 9. The other parameters of the forming process were given as follows:

- Isotropic elasticity: $E = 69$ GPa, $\nu = 0.33$,
- Isotropic hardening curve: $\bar{\sigma} = 646(0.025 + \bar{\epsilon})^{0.227}$ MPa,
- Coulomb coefficient of friction: 0.1,
- Blank holding force: 22.2 kN (5.55 kN for a quarter region).

The small friction coefficient simulates a well lubricated contact between blank and tools. Also, the force on the holder is small enough so that it does not add additional yielding in the material, but big enough to prevent the wrinkling of the blank.

Due to the orthotropic symmetry of the material, only a quarter of the blank was simulated. The typical mesh used on the blank is shown in Fig. 9. For plane stress analysis it consisted of one layer of continuum shell elements, SC8R, with 21 integration points across thickness (1806 nodes, 854 elements), whereas for 3D analysis it consisted of five layers of linear continuum (brick) elements, C3D8R (5418 nodes, 4270 elements). For 3D analyzes, the two coefficients k13 and k23 in (76) were computed using data for yielding in simple shear:

$$k_{13} = 0.5(\sigma_0/\sigma_{xz})^2 = 0.5(\bar{\sigma}_{xz})^{-2}, \quad k_{23} = 0.5(\sigma_0/\sigma_{yz})^2 = 0.5(\bar{\sigma}_{yz})^{-2} \tag{77}$$

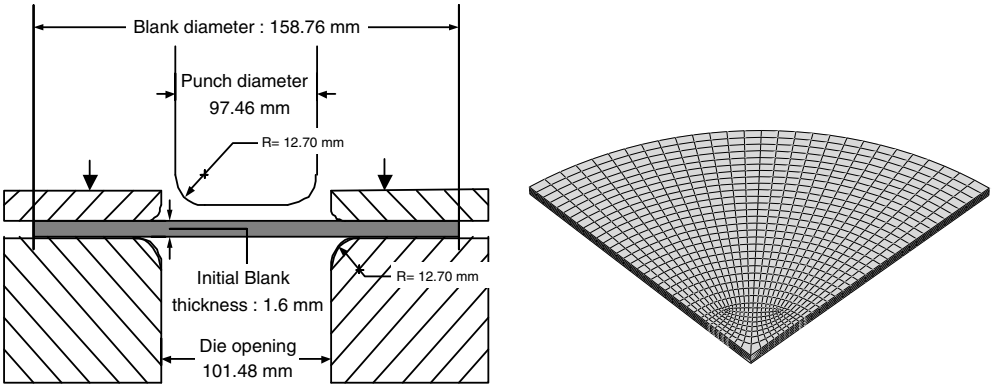

Fig. 9. Geometrical setting and tool dimensions for the drawing with cylindrical punch simulation (left), and typical mesh used on the blank (right).

Since these data are difficult to obtain for thin sheets by using mechanical tests, one can estimate it using polycrystal simulations based on texture data. This approach has been adopted in Barlat et al. (2005), where it is found that $\bar{\sigma}_{xz} = \bar{\sigma}_{yz} = 0.47$, for AA2090-T3. Then $k_{13} = k_{23} = 2.2635$.

Fig. 10 presents the profiles of the final cup for plane stress and 3D Poly4 simulations and comparison with Yld96 profile. The in plane material coefficients we used are those listed in Table 2 for AA2090-T3. Three observations are important to be made here. First, as expected, the difference between the plane stress and 3D analyzes is very small. The 2D and 3D profiles differ only in the vicinity of the 0°, 90°, 180° and 270° directions. The same trend is also observed in all the other simulations, for Poly6 and Poly8. This is due to the small holding force. Second, the overall height prediction of Poly4-profile is good, and does not have the height mismatch of the Yld96-profile which predicts a smaller height of the cup in the rolling direction than in the transverse direction, in contradiction with the experimental trend. Third, the Poly4-profile has eight ears, whereas the experimental profile shows six: four big ears located at 45°, 135°, 225° and 315° from rolling, and two (very) small ears symmetrically located along the rolling direction. The two extra ears of the Poly4-profile are symmetrically located along the transverse direction. This is due to the incomplete Poly4 description of the *r*-value variation. Further detail on this matter will be brought in the following section.

In Fig. 11 the profiles for the Poly6 and Poly8 3D-simulations are shown, together with the Yld2004-profile obtained from Yoon et al. (2006). The AA2090- T3 in-plane coefficients used for Poly6 are those in Table 3 and for Poly8 those in Table 4. The overall Poly6 and Poly8 profile predictions are very good (correct height and correct positioning and number of ears, six) and differ very little from the Yld2004 profile. This difference might come from the different finite element used in the cited paper. The difference between the Poly6 and Poly8 profiles is almost negligible. This shows that a correct description of the anisotropic plastic properties is sufficient in order to obtain the correct profile, and thus the predicted profile is yield-criterion-independent.

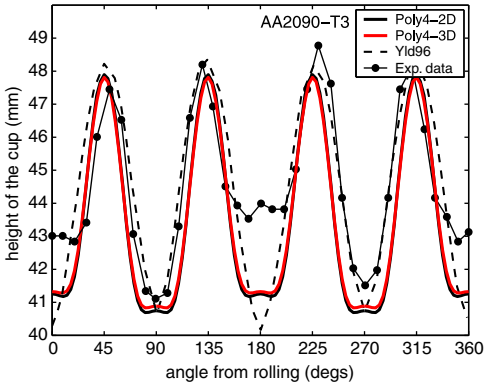

Fig. 10. Profiles of AA2090-T3 drawn cups simulated with Poly4, 2D and 3D. Yld96 simulation is also shown, data after Yoon et al. (2006).

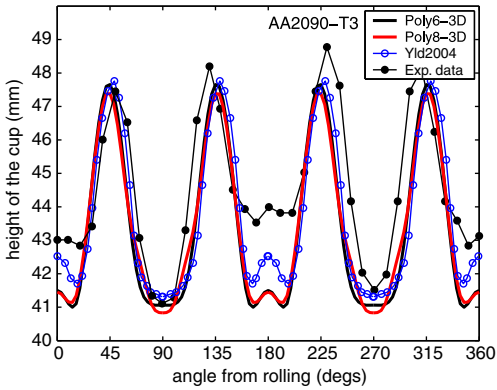

Fig. 11. Profiles of AA2090-T3 drawn cups simulated with Poly6-3D and Poly8-3D. Yld2004 simulation is also shown, data after Yoon et al. (2006).

7. Discussion and further examples

To explain the location of the ears (and hollows) on the rim of the cup in the deep drawing problem, Hill (1950, pp. 330–331) advances the hypothesis that, assuming isotropic hardening and plane stress conditions, the ears begin to develop at those locations on the rim where the strain increment has the radial direction as principal direction. Since at the rim only the hoop stress is non-zero (compressive), this hypothesis implies that ears begin to grow at those locations on the rim where the stress and strain increment tensors have the same principal directions. Hill then proves that those radial directions where the stress and strain increment are collinear are completely determined by the locations of the stationary points of the directional yield strength. Indeed, for a uniaxial tensile test at an angle θ from the rolling direction we have $\bar{\sigma}(\theta) = f^{-1}(\cos^2\theta, \sin^2\theta, \cos\theta\sin\theta)$ and then the equation $\mathrm{d}\bar{\sigma}/\mathrm{d}\theta = 0$ is equivalent with

$$\frac{\partial f}{\partial \sigma_x}\frac{\mathrm{d}\sigma_x}{\mathrm{d}\theta} + \frac{\partial f}{\partial \sigma_y}\frac{\mathrm{d}\sigma_y}{\mathrm{d}\theta} + 2\frac{\partial f}{\partial \sigma_{xy}}\frac{\mathrm{d}\sigma_{xy}}{\mathrm{d}\theta} = 0 \tag{78}$$

which can be further transformed into the equality

$$\frac{\cos^2\theta - \sin^2\theta}{2\sin\theta\cos\theta} = \frac{\partial f/\partial\sigma_x - \partial f/\partial\sigma_y}{2\partial f/\partial\sigma_{xy}} \iff \frac{\sigma_x - \sigma_y}{2\sigma_{xy}} = \frac{d\epsilon_x - \mathrm{d}\epsilon_y}{2\mathrm{d}\epsilon_{xy}} \tag{79}$$

if one neglects the elastic part from the strain increment. The last equality ex- presses the condition for the stress and strain increment tensors to be collinear. Next, an infinitesimal element at the rim at an angle θ from the rolling direction is in a state of uniaxial compression along the hoop direction. Since the yield function is assumed orthotropic and symmetric with respect to tension compression yielding properties, it follows that the locations where ears and hollows develop (stress and strain increment are collinear) are at $90^\circ - \theta_i$, where θ_i are the stationary directions of the directional yield strength. In particular, due to the orthotropic symmetry, the $\theta = 0^\circ$ and $\theta = 90^\circ$ directions are always stationary points for the directional yield strength and therefore the above theory predicts that cups drawn from orthotropic blanks always have ears or hollows at 0° and 90°. This

is confirmed by virtually all experimental profiles of drawn cylindrical cups, and it also explains the hollows along the rolling and transverse directions for the square cup problem.

However, the above theory does not precisely predict whether a ear or a hollow will develop at the corresponding location. In Fig. 12 the evolution of the topology of the rim during cup drawing simulation is shown for AA2090-T3 sheet, where the distance between the points on the rim and the center of the bottom of the cup is plotted versus the angle from rolling. The four big ears at 45°,135°, 225°, and 315° start developing right from the beginning of the drawing process, whereas the small ears at 0° and 180° begin to grow only after about 20% of punch travel. Even more, between 40% and 70% punch travel, the profile has eight ears, with two very small ears added along the transverse direction (TD). Thus, the topology of the profile is not fixed during the drawing process, which shows the important influence of hardening in the material, or, in a first approximation, of the flow anisotropy (r-value). At the extreme case, the theory will make no prediction about earing if the directional yield strength of the material is uniform while the r-value is still anisotropic (more precisely, the theory predicts that ears could develop at any location). For example, one can imagine a material, called here Mat_1, with constant directional yield strength (data: $\bar{\sigma}_{\theta j} = 1.0, j = 1, \ldots, 7, \bar{\sigma}_b = 1.0$), and r-value variation identical with the one of AA2090-T3, including the biaxial value. Poly6 modeling of this material is shown in Figs. 13 and 14, where the data fit for the directional yield strength and r-values, and its corresponding yield surface are drawn. Table 3 lists the corresponding coefficients of Poly6 for Mat_1. The predicted directional yield strength for Mat_1 is virtually constant (with a variation less than 0.0005), whereas the biaxial predictions for Mat_1 are $\bar{\sigma}_b = 1.000, r_b = 0.662$. At the same time, if a cylindrical cup is drawn from a Mat_1 sheet, in the same conditions as for AA2090-T3 (geometry, friction, blank holding force, etc), one obtains the earing profile shown in Fig. 15. The predicted profile of Mat_1 has eight ears located at 0°,45°,90°,135°, etc, with respect to the rolling direction. This result again underlines the influence of the directional variation of the r-value on the location of the ears and hollows.

After careful examinations of many experimental data for yield strength and r-value and their corresponding profiles, Yoon et al. (2006) reach the conclusion that the r-value data are in general responsible for the shape of the profile, while the variation of the yield

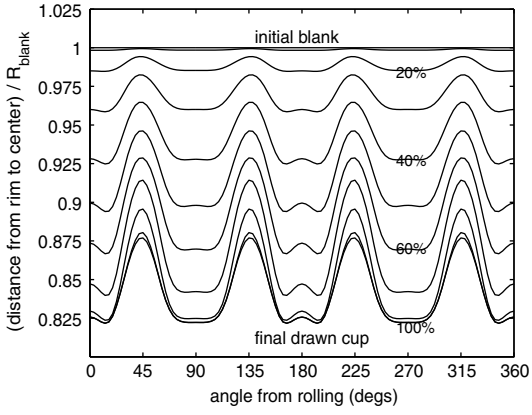

Fig. 12. Evolution of the profile of the cup during drawing process of AA2090-T3 simulated with Poly6.

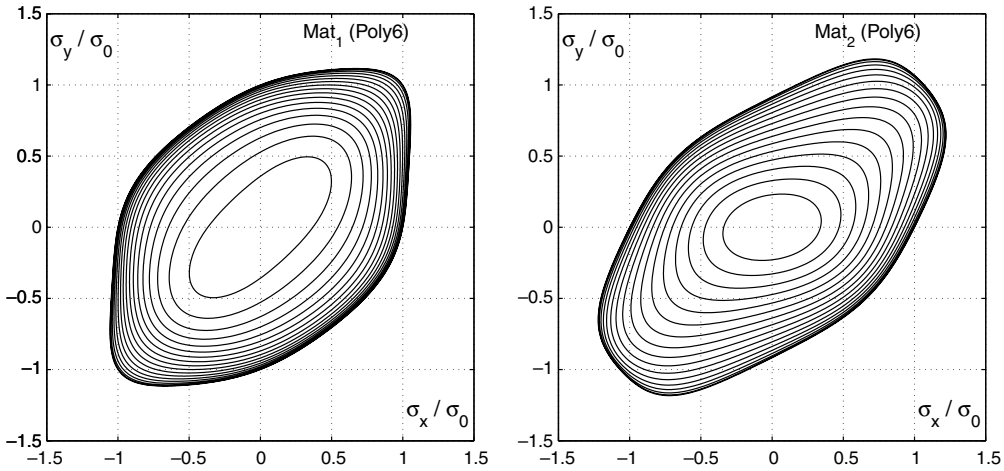

Fig. 13. Projections on the biaxial plane of the Poly6 yield surfaces for Mat_1 (left) and Mat_2 (right).

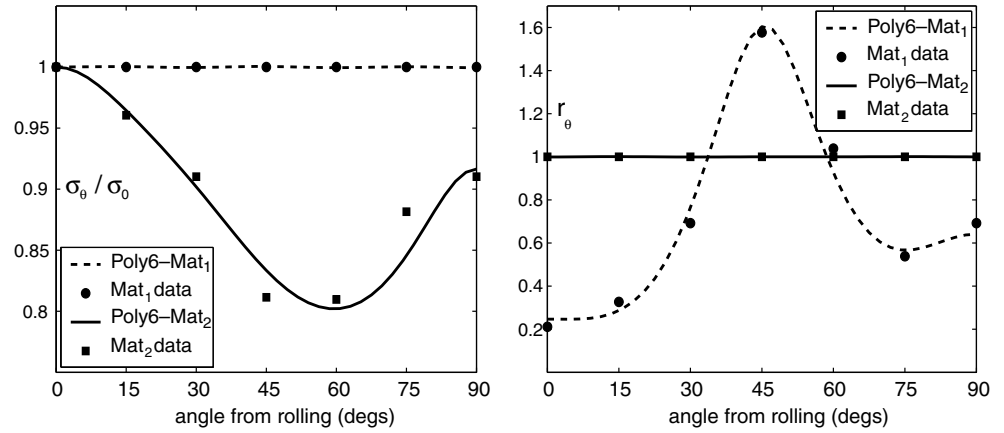

Fig. 14. Poly6 material characterization of Mat_1 and Mat_2: Directional yield strength (left) and r-value (right).

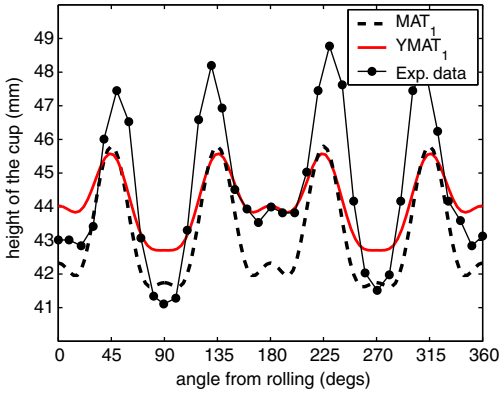

Fig. 15. Profiles of fictitious material MAT_1 cup as predicted by Poly6 (FEM), and by analytical formula (81) proposed by Yoon et al. (2006). For comparison purposes, the experimental profile of AA2090-T3 is also shown.

strength dictates the magnitude of the ears. A closer look at the predicted profile for Mat_1 on the interval [0°, 90°] reveals that, with the exception of the small ear at 90°, the shape of the profile is approximately a mirror image of the r-value variation on [0°, 90°]. The same correlation seems to be true for the profile of AA2090-T3 also. In the cited paper, Yoon and his coworkers went one step further and proposed a quantitative formula that connects the variation of the r-value with the height of the profile. It is based on the same observation as in Hill's theory that an infinitesimal element along the circumferential direction, while on the die, is basically in a state of uniaxial compression parallel with the circumferential direction (this assumption becomes less accurate as the element approaches the shoulder of the die where a uniaxial tension along the radial direction is also added due to the pulling of the punch). Then, assuming the same properties in tension and compression, the following formula holds true, Chung et al. (1996)

$$r_{\theta+90} = \frac{\epsilon_r}{\epsilon_t} = \frac{-\epsilon_r}{\epsilon_r + \epsilon_\theta} \tag{80}$$

where ϵ_r, ϵ_θ and ϵ_t are the strain in the radial, circumferential and thickness directions, and in the right member of the above equation use of the incompressibility of the strain increment has been made (the elastic part of strain is neglected). Let R_c and R_b denote the radii of the cup and of the blank. Then a ring of radius R, with $R_c \leqslant R \leqslant R_b$, is compressed to the radius R_c in the final drawn cup, and therefore one can approximate the circumferential strain for this ring with $\epsilon_\theta = \ln(R_c/R)$. Solving for ϵ_r in Eq. (80), the height of the cup is then obtained in the form (Yoon et al., 2006):

$$\begin{aligned} H(\theta) &= r_p + (R_b - R_c) + \int_{R_d}^{R_b} \epsilon_r \, dR \\ &= r_p + (R_b - R_c) + \frac{R_b r_{\theta+90}}{1 + r_{\theta+90}} [\ln(R_b/R_c) + R_c/R_b - 1] \end{aligned} \tag{81}$$

where r_p denotes the radius of the punch shoulder. The term $r_p + (R_b - R_c)$ corresponds to the "initial" height of the cup, the one that would be obtained by pure rigid motion (an ideal bending of the blank into a cup).

Formula (81) is entirely based on r-value data and therefore one cannot expect it to output accurate quantitative profile prediction. However, it is proposed as a quick and inexpensive predictor of the shape (or topology) of the profile. But, as we have remarked previously, the topology of the profile can change during the drawing process and, even if the measured r-value also includes some information about the hardening in the material, this change cannot be entirely explained only by r-value data. Furthermore, if Poly6 prediction for MAT_1 r-value is used in formula (81), we obtain the profile marked as YMAT_1 in Fig. 15. YMAT_1 has six ears and it is a prediction for both AA2090-T3 and MAT_1 profiles, since they have the same r-value description by Poly6. At the same time, the difference between the shape of the AA2090-T3 sheet FE profile, Poly6 curve in Fig. 11, and that of MAT_1 Poly6 FE profile in Fig. 15 is clear: one has six ears, the other has eight. This difference can be again pushed at extreme by considering an imaginary material that has uniform directional r-value (data: $r_b = r_{\theta j} = 1.000, j = 1, \ldots, 7$), and yield strength variation identical with the one of AA2090-T3, including the biaxial value. Poly6 description of this fictitious material called MAT_2 is listed in Table 3 and plotted in Figs. 13 and 14. Poly6 biaxial predictions for Mat_2 are $\bar{\sigma}_b = 1.035, r_b = 1.000$. Now, if a MAT_2

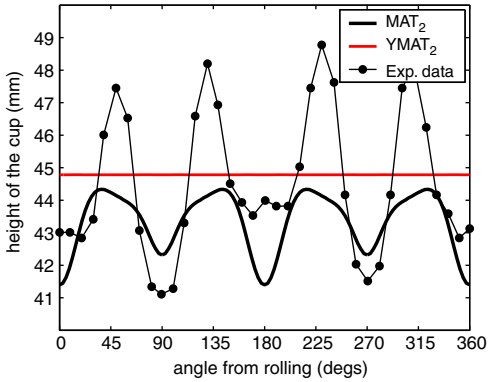

Fig. 16. Profiles of fictitious material MAT_2 cup as predicted by Poly6 (FEM), and by analytical formula (81) proposed by Yoon et al. (2006). For comparison purposes, the experimental profile of AA2090-T3 is also shown.

sheet is drawn in identical conditions as for the AA2090-T3 sheet in the previous section, the final cup will have the profile plotted in Fig. 16. In the same figure is plotted the $YMAT_2$ profile predicted by formula (81) if the Poly6 description for MAT_2 r-value is used as input. The topological difference between the two profiles is self-evident: The $YMAT_2$ profile is uniform, while the FE Poly6 MAT_2 profile has four big ears.

It follows then from the above discussion that an accurate theory of earing in deep drawn cups from metallic sheets with anisotropic yielding properties, must take into account both the directional variation of the yield strength and r-value, and also the hardening law of the material.

8. Conclusions

Homogeneous polynomials of fourth, sixth and eighth-order were investigated in this paper as orthotropic yield functions. For the fourth-order polynomial, Poly4, necessary conditions for the yield surface to be real-valued and convex were derived in simple analytic form. Although not proven here, this conditions were also sufficient for the particular applications presented. Compared with the initial identification formulas of Gotoh (1977), improved analytic formulas for the coefficients of Poly4 were also proposed. For sixth, Poly6, and eighth, Poly8, order polynomials we proposed a general constrained optimization procedure to identify the material coefficients such that the resulting yield surfaces are real-valued and convex. Poly4 brings a significant improvement over Hill's quadratic criterion, and is comparable to Yld96, being capable of simultaneous description of yield strength and r-value. However, as for Hill's quadratic and Yld96, Poly4 is recommended to be used only at the description of mild anisotropic properties, since incomplete characterization of the plastic anisotropy can lead to less accurate results in FE simulations. For strong anisotropic properties in yielding, like those of AA2090-T3, Poly6 and Poly8 are recommended.

A simple methodology for extending plane stress yield functions to 3D yield functions was also described. The 2D polynomial yield functions and their 3D extensions were applied to the simulation of two deep drawing processes: square and cylindrical cup forming. It was proven that accurate descriptions of both the yield strength and r-value

directional variations are the necessary conditions for the accurate prediction of the earing profile of cylindrical cups. They are also sufficient, for we have shown that three different yield functions, Poly6, Poly8, and Yld2004, with almost identical description of the data, predict almost identical profiles.

Appendix 1

The unit circle in the plane $\sigma_y = 0$ is parameterized in the form $\sigma_x = \cos\omega$ and $\sigma_{xy} = \sin\omega$. The restriction of P_4 to this circle is then

$$P_4(\omega) = a_1\cos^4\omega + a_6\cos^2\omega\sin^2\omega + a_9\sin^4\omega \tag{A.1}$$

and Eq. (9) becomes

$$g(\omega, a_6) := Aa_6^2 + Ba_6 + C \geqslant 0 \quad (\forall)\omega \in [0, 2\pi) \tag{A.2}$$

where

$$\begin{aligned} A &:= -4\cos^2\omega\sin^2\omega \leqslant 0 \quad (\forall)\omega \in [0, 2\pi) \\ B &:= 8(a_1\cos^4\omega + a_9\sin^4\omega) > 0 (\forall)\omega \in [0, 2\pi) \\ C &:= 48a_1a_9\cos^2\omega\sin^2\omega \geqslant 0 \quad (\forall)\omega \in [0, 2\pi) \end{aligned} \tag{A.3}$$

We note first that for $\omega = 0, \pi/2, \pi$, or $3\pi/2$ we have $A = C = 0$, and therefore we must have $a_6 \geqslant 0$. Excluding these cases, Eq. (A.2) is a quadratic inequality for a_6. Taking into account the signs of A, B and C we see that, for any fixed ω the equation $g(\omega, a_6) = 0$ always has two roots

$$x_1(\omega) := (-B/2 + \sqrt{\Delta})/A < 0 (-B/2 - \sqrt{\Delta})/A =: x_2(\omega) \tag{A.4}$$

where $\Delta := (B/2)^2 - AC > 0$. Thus, a_6 must satisfy

$$0 \leqslant a_6 \leqslant \min_{\omega\in[0,\pi]} x_2(\omega) \tag{A.5}$$

Solving for x_2 we obtain

$$x_2(\omega) = f(\omega) + [f^2(\omega) + k_6]^{1/2} \tag{A.6}$$

where $k_6 := 12a_1a_9$, and

$$f(\omega) := a_1 ctg^2\omega + a_9 tg^2\omega > 0 \tag{A.7}$$

The minimum value of $x_2(\omega)$ is attained for

$$\omega_6 := \text{arc}tg[(a_1/a_9)^{1/4}] \tag{A.8}$$

and finally we obtain for a_6:

$$0 \leqslant a_6 \leqslant f(\omega_6) + [f^2(\omega_6) + k_6]^{1/2} = 6\sqrt{a_1a_9} \tag{A.9}$$

An entirely similar reasoning leads to the second inequality in Eq. (24). For both restrictions of P_4 to the planes $\sigma_x = 0$ and $\sigma_y = 0$ the positivity condition is easily shown to reduce to weaker inequalities than $a_8 \geqslant 0$ and $a_6 \geqslant 0$, and therefore inequalities (24) are also sufficient for these two restrictions to be real-valued functions. Finally, after parameterizing the unit

circle in the plane $\sigma_x = \sigma_y$ in the form $\sigma_x = \sigma_y = (\cos\omega)/\sqrt{2}, \sigma_{xy} = \sin\omega, \omega \in [0, 2\pi)$, and assuming that we have $a_6 + a_7 + a_8 = B_5$, the restriction of P_4 to this circle is expressed as

$$P_4(\omega) = (1/4)[B_1\cos^4\omega + 2B_5\cos^2\omega\sin^2\omega + 4a_9\sin^4\omega] \tag{A.10}$$

This expression is similar with the one in Eq. (A.1), and thus:

$$0 \leqslant B_5 \leqslant 6\sqrt{B_1 a_9} \tag{A.11}$$

Recalling from Eq. (22) the definition of B_5, we then obtain the following two inequalities

$$2B_1 \leqslant \frac{(2/\bar{\sigma}_{45})^4}{1 + r_{45}} \leqslant 2B_1 + b\sqrt{a_9 B_1} \tag{A.12}$$

The left-hand side inequality in (A.12) gives the following bound on r_{45}

$$r_{45} \leqslant t/2 - 1 \tag{A.13}$$

where we have denoted $t := (2/\bar{\sigma}_{45})^4/B_1 = (2\bar{\sigma}_b/\bar{\sigma}_{45})^4$. Using the formula for a_9, Eq. (21), and after some algebra, the right-hand side inequality of (A.12) is equivalent with

$$(9t + 8)r_{45}^2 + 2(5t + 8)r_{45} + 9 - (t/2 - 1)^2 \geqslant 0 \tag{A.14}$$

Regarding r_{45} as variable, the above inequality has the solution in the form $r_{45} \in (-\infty, x_1] \cup [x_2, +\infty)$, where x_i are the roots of the associated equation. Since $x_1 < 0$ and $r_{45} > 0$, only the right-hand interval is accepted as solution. This leads to the bounds in Eq. (25).

Appendix 2

Let us consider the orthotropic fourth-order polynomial

$$P_4 = b_1\sigma_x^4 + b_2\sigma_x^3\sigma_y + b_3\sigma_x^2\sigma_y^2 + b_4\sigma_x\sigma_y^3 + b_5\sigma_y^4 + (b_6\sigma_x^2 + b_7\sigma_x\sigma_y + b_8\sigma_y^2)\sigma_{xy}^2 + b_9\sigma_{xy}^4$$

The coefficients of the eighth-order polynomial P_4^2 are presented. They can be used as initial guess for Poly8 coefficient identification. Thus, after identifying the coefficients in the equality $P_8 = P_4^2$, with P_8 given by (51), we obtain

$$\begin{aligned}
a_1 &= b_1^2 & a_{14} &= 2(b_8b_3 + b_5b_6 + b_7b_4)\\
a_2 &= 2b_2b_1 & a_{15} &= 2(b_8b_4 + b_5b_7)\\
a_3 &= 2b_3b_1 + b_2^2 & a_{16} &= 2b_8b_5\\
a_4 &= 2(b_4b_1 + b_3b_2) & a_{17} &= 2b_9b_1 + b_6^2\\
a_5 &= 2(b_4b_2 + b_5b_1) + b_3^2 & a_{18} &= 2(b_9b_2 + b_7b_6)\\
a_6 &= 2(b_5b_2 + b_4b_3) & a_{19} &= 2(b_9b_3 + b_8b_6) + b_7^2\\
a_7 &= 2b_5b_3 + b_4^2 & a_{20} &= 2(b_9b_4 + b_8b_7)\\
a_8 &= 2b_5b_4 & a_{21} &= 2b_9b_5 + b_8^2\\
a_9 &= b_5^2 & a_{22} &= 2b_9b_6\\
a_{10} &= 2b_6b_1 & a_{23} &= 2b_9b_7\\
a_{11} &= 2(b_7b_1 + b_6b_2) & a_{24} &= 2b_9b_8\\
a_{12} &= 2(b_6b_3 + b_7b_2 + b_8b_1) & a_{25} &= b_9^2\\
a_{13} &= 2(b_8b_2 + b_7b_3 + b_4b_6)
\end{aligned}$$

References

Arminjon, M., Bacroix, B., Imbault, D., Raphanel, J.L., 1994. A fourth-order plastic potential for anisotropic metals and its analytical calculation from texture function. Acta Mech. 107, 33.

Barlat, F., Maeda, Y., Chung, K., Yanagawa, M., Brem, J.C., Hayashida, Y., Lege, D.J., Matsui, K., Murtha, S.J., Hattori, S., Becker, R.C., Makosey, S., 1997. Yield function development for aluminum alloy sheets. J. Mech. Phys. Solids 45, 1727.

Barlat, F., Aretz, H., Yoon, J.W., Karabin, M.E., Brem, J.C., Dick, R.E., 2005. Linear transformation based anisotropic yield function. Int. J. Plast. 21, 1009.

Barlat, F., Yoon, J.W., Cazacu, O., 2007. On linear transformations of stress tensors for the description of plastic anisotropy. Int. J. Plasticity 23, 876.

Chung, K., Lee, S.Y., Barlat, F., Keum, Y.T., Park, J.M., 1996. Finite element simulation of sheet forming based on a planar anisotropic strain-rate potential. Int. J. Plasticity 12, 93.

Danckert, J., 1995. Experimental investigation of a square-cup deep drawing process. J. Mat. Proc. Technol. 50, 375.

Dawson, P.R., MacEwen, S.R., Wu, P.D., 2003. Advances in sheet metal forming analyses: dealing with mechanical anisotropy from crystallographic texture. Int. Mat. Rev. 28, 86.

Gotoh, M., 1977. A theory of plastic anisotropy based on a yield function of fourth order (plane stress) - part I and II. Int. J. Mech. Sci. 19, 505.

Groemer, H., 1996. Geometric Applications of Fourier Series and Spherical Harmonics. Cambridge University Press.

Hill, R., 1950. The Mathematical Theory of Plasticity. Clarendon Press, Oxford.

Hosford, W.F., 1972. A generalized isotropic yield criterion. J. Appl. Mech. Trans. ASME 39, 607.

Pearce, R., 1968. Some aspects of anisotropic plasticity in sheet metals. Int. J. Mech. Sci. 10, 995.

Savoie, J., MacEwen, S.R., 1995. A sixth order inverse potential function for incorporation of crystallographic texture into predictions of properties of aluminium sheet. Texture Microstruct. 26–27, 495.

Schitkowski, K., 1986. NLPQL: a Fortran subroutine solving constrained non-linear programming problems. Ann. Oper. Res. 5, 485.

Shephard, G.C., 1968. A uniqueness theorem for the Steiner point of a convex region. J. London Math. Soc. 43, 439.

Simo, J.C., Hughes, T.J.R., 1999. Computational Inelasticity. Springer Verlag, Berlin.

Tugcu, P., Neale, K.W., 1999. On the implementation of anisotropic yield functions into finite strain problems of sheet metal forming. Int. J. Plasticity 15, 1021.

Wu, P.D., Jain, M., Savoie, J., MacEwen, S.R., Tugcu, P., Neale, K.W., 2003. Evaluation of anisotropic yield functions for aluminum sheets. Int. J. Plasticity 19, 121.

Yoon, J.W., Barlat, F., Chung, K., Pourboghrat, F., Yang, D.Y., 2000. Earing prediction based on asymmetric nonquadratic yield function. Int. J. Plasticity 16, 1105.

Yoon, J.W., Barlat, F., Dick, R.E., Karabin, M.E., 2006. Prediction of six or eight ears in a drawn cup based on a new anisotropic yield function. Int. J. Plasticity 22, 174.

Zhou, Y., Jonas, J.J., Savoie, J., Makinde, A., MacEwen, S.R., 1998. Effect of texture on earing in fcc metals: finite element simulations. Int. J. Plasticity 14, 117.